Production of $\psi(4040)$, $\psi(4160)$, and $\psi(4415)$ mesons in hadronic matter

Li-Yuan Li,[1] Xiao-Ming Xu,[1] and H. J. Weber[2]

[1]*Department of Physics, Shanghai University, Baoshan, Shanghai 200444, China*
[2]*Department of Physics, University of Virginia, Charlottesville, Virginia 22904, USA*

(Received 7 February 2022; accepted 23 May 2022; published 17 June 2022)

We present the first study of production of $\psi(4040)$, $\psi(4160)$, and $\psi(4415)$ mesons in hadronic matter. Quark interchange between two colliding charmed mesons leads to the production of the three mesons. We calculate unpolarized cross sections for the reactions $D\bar{D} \to \rho R$, $D\bar{D}^* \to \pi R$, $D\bar{D}^* \to \rho R$, $D^*\bar{D} \to \pi R$, $D^*\bar{D} \to \rho R$, $D^*\bar{D}^* \to \pi R$, and $D^*\bar{D}^* \to \rho R$, where R stands for $\psi(4040)$, $\psi(4160)$, and $\psi(4415)$. In the temperature region covering hadronic matter, the peak cross sections of producing $\psi(4040)$ are similar to or larger than the ones of producing $\psi(4415)$, and the latter are generally larger than those of producing $\psi(4160)$. With the cross sections, we establish new master rate equations for $\psi(4040)$, $\psi(4160)$, and $\psi(4415)$. The equations are solved for central Pb-Pb collisions at $\sqrt{s_{NN}} = 5.02$ TeV at the Large Hadron Collider. Solutions of the equations show that the $\psi(4040)$ number density at kinetic freeze-out of hadronic matter is larger than the $\psi(4415)$ number density, which is larger than the $\psi(4160)$ number density.

DOI: 10.1103/PhysRevD.105.114025

I. INTRODUCTION

The masses, decay widths, and decay modes of $\psi(4040)$, $\psi(4160)$, and $\psi(4415)$ mesons produced in e^+e^- collisions have been measured by the Mark I [1], DASP [2], BES [3], CLEO [4], Belle [5], *BABAR* [6], and BES III [7] Collaborations. The three charmonia have also been studied in the $B^+ \to K^+\mu^+\mu^-$ decay and the $B^+ \to D^+D^-K^+$ decay by the LHCb Collaboration [8]. In meson degrees of freedom, an electron-positron collision produces one photon, and the photon then converts into $\psi(4040)$, $\psi(4160)$, or $\psi(4415)$ [9,10]. In quark degrees of freedom the photon produced in the electron-positron annihilation splits into a charm quark and a charm antiquark which evolve nonperturbatively into $\psi(4040)$, $\psi(4160)$, or $\psi(4415)$ with certain probabilities.

It is shown in Refs. [11–13] that $\psi(4040)$, $\psi(4160)$, and $\psi(4415)$ can be individually interpreted as the 3^3S_1, 2^3D_1, and 4^3S_1 quark-antiquark states. In ultrarelativistic heavy-ion collisions, the three states created in initial nucleus-nucleus collisions are dissolved in quark-gluon plasmas [14]. At the critical temperature, hadronization of the quark-gluon plasma gives hadronic matter that evolves until kinetic freeze-out. All possible hadron-hadron scattering occurs in hadronic matter, and various quark processes appear during scattering [15]. Quark interchange between two colliding charmed mesons in hadronic matter leads to production of $\psi(4040)$, $\psi(4160)$, and $\psi(4415)$, for example, $D\bar{D}^* \to \rho\psi(4040)$, $\rho\psi(4160)$, and $\rho\psi(4415)$. Therefore, the three charmonia can be produced in hadronic matter.

In the present work, we study the production of $\psi(4040)$, $\psi(4160)$, and $\psi(4415)$ via quark interchange between two colliding charmed mesons in hadronic matter. Since the temperature of hadronic matter varies during its expansion, we need to study temperature dependence of cross sections for the production of the three charmonia. Furthermore, we establish new master rate equations to account for charmonium number densities that result from the reactions of charmed mesons. Number densities are obtained from the equations for central Pb-Pb collisions at the center-of-mass energy per nucleon-nucleon pair $\sqrt{s_{NN}} = 5.02$ TeV at the Large Hadron Collider (LHC).

This paper is organized as follows. In Sec. II we provide cross section formulas for two-to-two scattering of charmed mesons. In Sec. III we give master rate equations for $\psi(4040)$, $\psi(4160)$, and $\psi(4415)$ mesons. In Sec. IV we show numerical cross sections and number densities of the three mesons produced in hadronic matter. Relevant discussions are given. In Sec. V we summarize the present work.

II. FORMALISM FOR $c\bar{c}$ PRODUCTION IN MESON-MESON COLLISIONS

Production of $\psi(4040)$, $\psi(4160)$, and $\psi(4415)$ mesons in hadronic matter concerns the reaction $A(c\bar{q}_2) + B(q_1\bar{c}) \to C(q_1\bar{q}_2) + D(c\bar{c})$ where c is a charm quark,

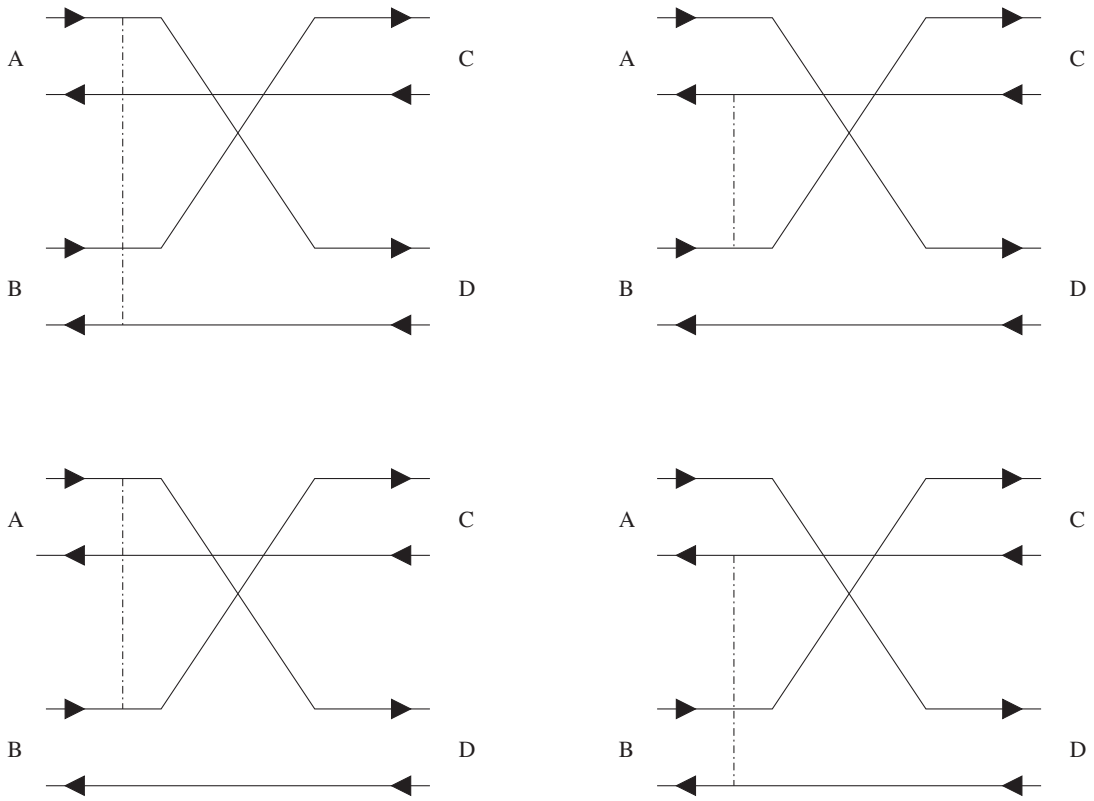

FIG. 1. Scattering in the prior form. Solid lines with triangles right (left) represent quarks (antiquarks). Dot-dashed lines indicate interactions.

q_1 is a light quark, and $\bar{q}_2$ is a light antiquark. This reaction is caused by interchange of c and q_1 between mesons A and B. Denote the spin of meson A (B, C, D) by S_A (S_B, S_C, S_D) and its magnetic projection quantum number by S_{Az} (S_{Bz}, S_{Cz}, S_{Dz}). The wave function of mesons A and B is

$$\psi_{AB} = \phi_{A\mathrm{rel}}\phi_{B\mathrm{rel}}\phi_{A\mathrm{color}}\phi_{B\mathrm{color}}\chi_{S_A S_{Az}}\chi_{S_B S_{Bz}}\varphi_{AB\mathrm{flavor}}, \quad (1)$$

and the wave function of mesons C and D is

$$\psi_{CD} = \phi_{C\mathrm{rel}}\phi_{D\mathrm{rel}}\phi_{C\mathrm{color}}\phi_{D\mathrm{color}}\chi_{S_C S_{Cz}}\chi_{S_D S_{Dz}}\varphi_{CD\mathrm{flavor}}, \quad (2)$$

where $\phi_{A\mathrm{rel}}$ ($\phi_{B\mathrm{rel}}$, $\phi_{C\mathrm{rel}}$, $\phi_{D\mathrm{rel}}$), $\phi_{A\mathrm{color}}$ ($\phi_{B\mathrm{color}}$, $\phi_{C\mathrm{color}}$, $\phi_{D\mathrm{color}}$), and $\chi_{S_A S_{Az}}$ ($\chi_{S_B S_{Bz}}$, $\chi_{S_C S_{Cz}}$, $\chi_{S_D S_{Dz}}$) are the mesonic quark-antiquark relative-motion wave function, color wave function, and spin wave function of meson A (B, C, D), respectively; the flavor wave function $\varphi_{AB\mathrm{flavor}}$ of mesons A and B possesses the same isospin as the flavor wave function $\varphi_{CD\mathrm{flavor}}$ of mesons C and D.

Two forms are involved in the Born-order meson-meson scattering in the quark interchange mechanism [16]. Scattering in the prior form as seen in Fig. 1 means that gluon exchange takes place prior to quark interchange. Scattering in the post form shown in Fig. 2 means quark interchange is followed by gluon exchange. In the two figures, the interaction between constituents a and b is indicated by the dot-dashed line, and its potential is V_{ab}. Scattering in the prior form needs interactions between the two constituents of meson A and the ones of meson B, which are described by the potentials $V_{c\bar{c}}$, $V_{\bar{q}_2 q_1}$, V_{cq_1}, and $V_{\bar{q}_2\bar{c}}$. The transition amplitude for scattering in the prior form is

$$\mathcal{M}_{\mathrm{fi}}^{\mathrm{prior}} = \sqrt{2E_A 2E_B 2E_C 2E_D}\int\frac{d^3p_{q_1\bar{q}_2}}{(2\pi)^3}\int\frac{d^3p_{c\bar{c}}}{(2\pi)^3}\psi_{CD}^{+} \times [V_{c\bar{c}}(\vec{p}\,'_c - \vec{p}_c) + V_{\bar{q}_2 q_1}(\vec{p}\,'_{\bar{q}_2} - \vec{p}_{\bar{q}_2}) + V_{cq_1}(\vec{p}\,'_c - \vec{p}_c) + V_{\bar{q}_2\bar{c}}(\vec{p}\,'_{\bar{q}_2} - \vec{p}_{\bar{q}_2})]\psi_{AB}, \quad (3)$$

where E_A (E_B, E_C, E_D) denotes the energy of meson A (B, C, D), and $\vec{p}_{ab}$ is the relative momentum of constituents a and b. The three-dimensional momentum of constituent a in the initial (final) mesons is labeled as $\vec{p}_a$ ($\vec{p}\,'_a$). Substituting Eqs. (1) and (2) in Eq. (3), we obtain

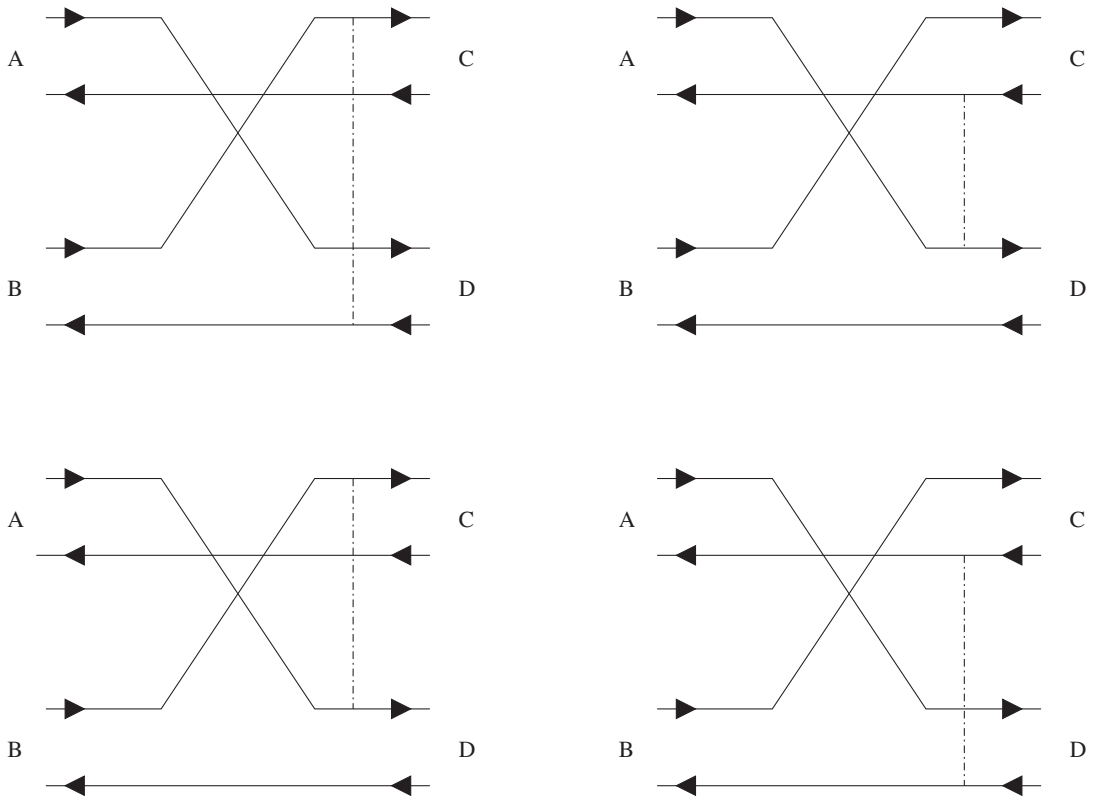

FIG. 2. Scattering in the post form. Solid lines with triangles right (left) represent quarks (antiquarks). Dot-dashed lines indicate interactions.

$$
\begin{aligned}
\mathcal{M}_{\mathrm{fi}}^{\mathrm{prior}} = & \sqrt{2E_A 2E_B 2E_C 2E_D}\varphi^{+}_{CD\mathrm{flavor}}\varphi_{AB\mathrm{flavor}}\phi^{+}_{C\mathrm{color}}\phi^{+}_{D\mathrm{color}}\chi^{+}_{S_C S_{C_z}}\chi^{+}_{S_D S_{D_z}} \\
& \times \left[\int \frac{d^3p_c}{(2\pi)^3}\frac{d^3p'_c}{(2\pi)^3}\phi^{+}_{C\mathrm{rel}}\left(\vec{p}_c - \vec{P} + \frac{m_{\bar{q}_2}}{m_{q_1}+m_{\bar{q}_2}}\vec{P}'\right)\phi^{+}_{D\mathrm{rel}}\left(\vec{p}'_c + \frac{m_c}{m_c+m_{\bar{c}}}\vec{P}'\right)\right. \\
& \times V_{c\bar{c}}(\vec{p}'_c - \vec{p}_c)\phi_{A\mathrm{rel}}\left(\vec{p}_c - \frac{m_c}{m_c+m_{\bar{q}_2}}\vec{P}\right)\phi_{B\mathrm{rel}}\left(\vec{p}_c - \frac{m_{\bar{c}}}{m_{q_1}+m_{\bar{c}}}\vec{P} + \vec{P}'\right) \\
& + \int \frac{d^3p_{\bar{q}_2}}{(2\pi)^3}\frac{d^3p'_{\bar{q}_2}}{(2\pi)^3}\phi^{+}_{C\mathrm{rel}}\left(-\vec{p}'_{\bar{q}_2} + \frac{m_{\bar{q}_2}}{m_{q_1}+m_{\bar{q}_2}}\vec{P}'\right)\phi^{+}_{D\mathrm{rel}}\left(-\vec{p}_{\bar{q}_2} + \vec{P} + \frac{m_c}{m_c+m_{\bar{c}}}\vec{P}'\right) \\
& \times V_{\bar{q}_2 q_1}(\vec{p}'_{\bar{q}_2} - \vec{p}_{\bar{q}_2})\phi_{A\mathrm{rel}}\left(-\vec{p}_{\bar{q}_2} + \frac{m_{\bar{q}_2}}{m_c+m_{\bar{q}_2}}\vec{P}\right)\phi_{B\mathrm{rel}}\left(-\vec{p}_{\bar{q}_2} + \frac{m_{q_1}}{m_{q_1}+m_{\bar{c}}}\vec{P} + \vec{P}'\right) \\
& + \int \frac{d^3p_c}{(2\pi)^3}\frac{d^3p'_c}{(2\pi)^3}\phi^{+}_{C\mathrm{rel}}\left(\vec{p}_c - \vec{P} + \frac{m_{\bar{q}_2}}{m_{q_1}+m_{\bar{q}_2}}\vec{P}'\right)\phi^{+}_{D\mathrm{rel}}\left(\vec{p}'_c + \frac{m_c}{m_c+m_{\bar{c}}}\vec{P}'\right) \\
& \times V_{cq_1}(\vec{p}'_c - \vec{p}_c)\phi_{A\mathrm{rel}}\left(\vec{p}_c - \frac{m_c}{m_c+m_{\bar{q}_2}}\vec{P}\right)\phi_{B\mathrm{rel}}\left(\vec{p}'_c - \frac{m_{\bar{c}}}{m_{q_1}+m_{\bar{c}}}\vec{P} + \vec{P}'\right) \\
& + \int \frac{d^3p_{\bar{q}_2}}{(2\pi)^3}\frac{d^3p'_{\bar{q}_2}}{(2\pi)^3}\phi^{+}_{C\mathrm{rel}}\left(-\vec{p}'_{\bar{q}_2} + \frac{m_{\bar{q}_2}}{m_{q_1}+m_{\bar{q}_2}}\vec{P}'\right)\phi^{+}_{D\mathrm{rel}}\left(-\vec{p}_{\bar{q}_2} + \vec{P} + \frac{m_c}{m_c+m_{\bar{c}}}\vec{P}'\right) \\
& \left. \times V_{\bar{q}_2\bar{c}}(\vec{p}'_{\bar{q}_2} - \vec{p}_{\bar{q}_2})\phi_{A\mathrm{rel}}\left(-\vec{p}_{\bar{q}_2} + \frac{m_{\bar{q}_2}}{m_c+m_{\bar{q}_2}}\vec{P}\right)\phi_{B\mathrm{rel}}\left(-\vec{p}'_{\bar{q}_2} + \frac{m_{q_1}}{m_{q_1}+m_{\bar{c}}}\vec{P} + \vec{P}'\right)\right] \\
& \times \chi_{S_A S_{A_z}}\chi_{S_B S_{B_z}}\phi_{A\mathrm{color}}\phi_{B\mathrm{color}}, \qquad (4)
\end{aligned}
$$

where m_a is the mass of constituent a; $\vec{P}$ and $\vec{P}'$ are the three-dimensional momenta of mesons A and C in the center-of-mass frame of the two initial mesons, respectively. The first, second, third, and fourth terms enclosed by the brackets correspond

to the upper left, upper right, lower left, and lower right diagrams in Fig. 1, respectively. Scattering in the post form needs interactions between the two constituents of meson C and the ones of meson D, which are described by the potentials $V_{q_1\bar{c}}$, $V_{\bar{q}_2 c}$, V_{cq_1}, and $V_{\bar{q}_2\bar{c}}$. The transition amplitude for scattering in the post form is

$$\mathcal{M}_{\rm fi}^{\rm post} = \sqrt{2E_A 2E_B 2E_C 2E_D}\int\frac{d^3p_{c\bar{q}_2}}{(2\pi)^3}\int\frac{d^3p_{q_1\bar{c}}}{(2\pi)^3}\psi^+_{CD} \times[V_{q_1\bar{c}}(\vec{p}\,'_{q_1}-\vec{p}_{q_1})+V_{\bar{q}_2 c}(\vec{p}\,'_{\bar{q}_2}-\vec{p}_{\bar{q}_2})+V_{cq_1}(\vec{p}\,'_c-\vec{p}_c)+V_{\bar{q}_2\bar{c}}(\vec{p}\,'_{\bar{q}_2}-\vec{p}_{\bar{q}_2})]\psi_{AB}. \tag{5}$$

With the wave functions of the initial mesons and the final mesons, we have

$$\begin{aligned}\mathcal{M}_{\rm fi}^{\rm post} = {}& \sqrt{2E_A 2E_B 2E_C 2E_D}\varphi^+_{CD\rm flavor}\varphi_{AB\rm flavor}\phi^+_{C\rm color}\phi^+_{D\rm color}\chi^+_{S_C S_{C\bar{z}}}\chi^+_{S_D S_{Dz}}\\ &\times\Bigg[\int\frac{d^3p_{q_1}}{(2\pi)^3}\frac{d^3p'_{q_1}}{(2\pi)^3}\phi^+_{C\rm rel}\left(\vec{p}\,'_{q_1}-\frac{m_{q_1}}{m_{q_1}+m_{\bar{q}_2}}\vec{P}'\right)\phi^+_{D\rm rel}\left(\vec{p}\,'_{q_1}+\vec{P}-\frac{m_{\bar{c}}}{m_c+m_{\bar{c}}}\vec{P}'\right)\\ &\times V_{q_1\bar{c}}(\vec{p}\,'_{q_1}-\vec{p}_{q_1})\phi_{A\rm rel}\left(\vec{p}\,'_{q_1}+\frac{m_{\bar{q}_2}}{m_c+m_{\bar{q}_2}}\vec{P}-\vec{P}'\right)\phi_{B\rm rel}\left(\vec{p}_{q_1}+\frac{m_{q_1}}{m_{q_1}+m_{\bar{c}}}\vec{P}\right)\\ &+\int\frac{d^3p_{\bar{q}_2}}{(2\pi)^3}\frac{d^3p'_{\bar{q}_2}}{(2\pi)^3}\phi^+_{C\rm rel}\left(-\vec{p}\,'_{\bar{q}_2}+\frac{m_{\bar{q}_2}}{m_{q_1}+m_{\bar{q}_2}}\vec{P}'\right)\phi^+_{D\rm rel}\left(-\vec{p}\,'_{\bar{q}_2}+\vec{P}+\frac{m_c}{m_c+m_{\bar{c}}}\vec{P}'\right)\\ &\times V_{\bar{q}_2 c}(\vec{p}\,'_{\bar{q}_2}-\vec{p}_{\bar{q}_2})\phi_{A\rm rel}\left(-\vec{p}_{\bar{q}_2}+\frac{m_{\bar{q}_2}}{m_c+m_{\bar{q}_2}}\vec{P}\right)\phi_{B\rm rel}\left(-\vec{p}\,'_{\bar{q}_2}+\frac{m_{q_1}}{m_{q_1}+m_{\bar{c}}}\vec{P}+\vec{P}'\right)\\ &+\int\frac{d^3p_c}{(2\pi)^3}\frac{d^3p'_c}{(2\pi)^3}\phi^+_{C\rm rel}\left(\vec{p}_c-\vec{P}+\frac{m_{\bar{q}_2}}{m_{q_1}+m_{\bar{q}_2}}\vec{P}'\right)\phi^+_{D\rm rel}\left(\vec{p}\,'_c+\frac{m_c}{m_c+m_{\bar{c}}}\vec{P}'\right)\\ &\times V_{cq_1}(\vec{p}\,'_c-\vec{p}_c)\phi_{A\rm rel}\left(\vec{p}_c-\frac{m_c}{m_c+m_{\bar{q}_2}}\vec{P}\right)\phi_{B\rm rel}\left(\vec{p}\,'_c-\frac{m_{\bar{c}}}{m_{q_1}+m_{\bar{c}}}\vec{P}+\vec{P}'\right)\\ &+\int\frac{d^3p_{\bar{q}_2}}{(2\pi)^3}\frac{d^3p'_{\bar{q}_2}}{(2\pi)^3}\phi^+_{C\rm rel}\left(-\vec{p}\,'_{\bar{q}_2}+\frac{m_{\bar{q}_2}}{m_{q_1}+m_{\bar{q}_2}}\vec{P}'\right)\phi^+_{D\rm rel}\left(-\vec{p}_{\bar{q}_2}+\vec{P}+\frac{m_c}{m_c+m_{\bar{c}}}\vec{P}'\right)\\ &\times V_{\bar{q}_2\bar{c}}(\vec{p}\,'_{\bar{q}_2}-\vec{p}_{\bar{q}_2})\phi_{A\rm rel}\left(-\vec{p}_{\bar{q}_2}+\frac{m_{\bar{q}_2}}{m_c+m_{\bar{q}_2}}\vec{P}\right)\phi_{B\rm rel}\left(-\vec{p}\,'_{\bar{q}_2}+\frac{m_{q_1}}{m_{q_1}+m_{\bar{c}}}\vec{P}+\vec{P}'\right)\Bigg]\\ &\times\chi_{S_A S_{Az}}\chi_{S_B S_{Bz}}\phi_{A\rm color}\phi_{B\rm color}. \end{aligned}\tag{6}$$

The first, second, third, and fourth terms enclosed by the brackets correspond to the upper left, upper right, lower left, and lower right diagrams in Fig. 2, respectively. In Eqs. (4) and (6), $\phi_{A\rm rel}$, $\phi_{B\rm rel}$, $\phi_{C\rm rel}$, and $\phi_{D\rm rel}$ are functions of $\vec{p}_{c\bar{q}_2}$, $\vec{p}_{q_1\bar{c}}$, $\vec{p}_{q_1\bar{q}_2}$, and $\vec{p}_{c\bar{c}}$, respectively. These relative momenta equal the expressions enclosed by the parentheses that follow $\phi_{A\rm rel}$, $\phi_{B\rm rel}$, $\phi_{C\rm rel}$, and $\phi_{D\rm rel}$. In Eqs. (3)–(6), $V_{c\bar{c}}$, $V_{\bar{q}_2 q_1}$, V_{cq_1}, $V_{\bar{q}_2\bar{c}}$, $V_{q_1\bar{c}}$, and $V_{\bar{q}_2 c}$ are momentum-space potentials that depend on momenta attached to the dot-dashed lines in Figs. 1 and 2. The momenta equal the expressions enclosed by the parentheses that follow $V_{c\bar{c}}$, $V_{\bar{q}_2 q_1}$, V_{cq_1}, $V_{\bar{q}_2\bar{c}}$, $V_{q_1\bar{c}}$, and $V_{\bar{q}_2 c}$.

As seen in Eqs. (4) and (6), each of $\mathcal{M}_{\rm fi}^{\rm prior}$ and $\mathcal{M}_{\rm fi}^{\rm post}$ contains four integrals. The first and second terms of $\mathcal{M}_{\rm fi}^{\rm prior}$ look different than the first and second terms of $\mathcal{M}_{\rm fi}^{\rm post}$, but the third and fourth terms of $\mathcal{M}_{\rm fi}^{\rm prior}$ are identical with the third and fourth terms of $\mathcal{M}_{\rm fi}^{\rm post}$. If the sum of the first and second terms of $\mathcal{M}_{\rm fi}^{\rm prior}$ does not equal the one of $\mathcal{M}_{\rm fi}^{\rm post}$, $\mathcal{M}_{\rm fi}^{\rm prior}$ does not equal $\mathcal{M}_{\rm fi}^{\rm post}$, and the post-prior ambiguity appears.

Denote by T the temperature and by $T_{\rm c}$ the critical temperature between quark-gluon plasmas and hadronic matter. Let $\vec{s}_a$ be the spin of constituent a. The mesonic quark-antiquark relative-motion wave functions $\phi_{\rm A\,rel}$, $\phi_{\rm B\,rel}$, $\phi_{\rm C\,rel}$, and $\phi_{\rm D\,rel}$ are the Fourier transform of the solutions of the Schrödinger equation with the potential between constituents a and b in coordinate space [17],

$$V_{ab}(\vec{r}_{ab}) = -\frac{\vec{\lambda}_a}{2}\cdot\frac{\vec{\lambda}_b}{2}\xi_1\left[1.3-\left(\frac{T}{T_c}\right)^4\right]\tanh(\xi_2 r_{ab}) + \frac{\vec{\lambda}_a}{2}\cdot\frac{\vec{\lambda}_b}{2}\frac{6\pi}{25}\frac{v(\lambda r_{ab})}{r_{ab}}\exp(-\xi_3 r_{ab})$$
$$-\frac{\vec{\lambda}_a}{2}\cdot\frac{\vec{\lambda}_b}{2}\frac{16\pi^2}{25}\frac{d^3}{\pi^{3/2}}\exp(-d^2 r_{ab}^2)\frac{\vec{s}_a\cdot\vec{s}_b}{m_a m_b} + \frac{\vec{\lambda}_a}{2}\cdot\frac{\vec{\lambda}_b}{2}\frac{4\pi}{25}\frac{1}{r_{ab}}\frac{d^2 v(\lambda r_{ab})}{dr_{ab}^2}\frac{\vec{s}_a\cdot\vec{s}_b}{m_a m_b}$$
$$-\frac{\vec{\lambda}_a}{2}\cdot\frac{\vec{\lambda}_b}{2}\frac{6\pi}{25 m_a m_b}\left[v(\lambda r_{ab}) - r_{ab}\frac{dv(\lambda r_{ab})}{dr_{ab}} + \frac{r_{ab}^2}{3}\frac{d^2 v(\lambda r_{ab})}{dr_{ab}^2}\right]$$
$$\times\left(\frac{3\vec{s}_a\cdot\vec{r}_{ab}\vec{s}_b\cdot\vec{r}_{ab}}{r_{ab}^5} - \frac{\vec{s}_a\cdot\vec{s}_b}{r_{ab}^3}\right), \tag{7}$$

where $\vec{r}_{ab}$ is the relative coordinate of constituents a and b; $\xi_1 = 0.525$, $\xi_2 = 1.5[0.75 + 0.25(T/T_c)^{10}]^6$, $\xi_3 = 0.6$, and $T_c = 0.175$ GeV, and $\lambda = \sqrt{25/16\pi^2\alpha'}$ with $\alpha' = 1.04\ \text{GeV}^{-2}$; v is a function of r_{ab} and is given by Buchmüller and Tye in Ref. [18]. The quantity d is related to constituent masses by

$$d^2 = d_1^2\left[\frac{1}{2} + \frac{1}{2}\left(\frac{4m_a m_b}{(m_a+m_b)^2}\right)^4\right] + d_2^2\left(\frac{2m_a m_b}{m_a+m_b}\right)^2, \tag{8}$$

where $d_1 = 0.15$ GeV and $d_2 = 0.705$. The short-distance part of the potential is obtained from perturbative quantum chromodynamics [18], and the temperature dependence is obtained from lattice gauge calculations [19]. The lattice calculations gave a temperature-dependent quark potential at intermediate and long distances. The potential at long distances has a distance-independent value that decreases with increasing temperature. The first term in Eq. (7) is the confining potential that corresponds to the lattice results. The expression $\frac{\vec{\lambda}_a}{2}\cdot\frac{\vec{\lambda}_b}{2}\frac{6\pi}{25}\frac{v(\lambda r_{ab})}{r_{ab}}$ in the second term arises from one-gluon exchange plus perturbative one- and two-loop corrections in vacuum [18], and the factor $\exp(-\xi_3 r_{ab})$ is a medium modification factor. The third term is the smeared spin-spin interaction that comes from one-gluon exchange between constituents a and b [11]. The fourth term is the spin-spin interaction that originates from perturbative one- and two-loop corrections to one-gluon exchange [20]. The fifth term is the tensor interaction that arises from one-gluon exchange plus perturbative one- and two-loop corrections [20].

In Fig. 3 we plot the central spin-independent potential, which is the sum of the first and second terms on the right-hand side of Eq. (7), the spin-spin interaction which is the sum of the third and fourth terms, the tensor interaction, and the potential $V_{c\bar{c}}$ between the charm quark and the charm antiquark inside the $\psi(4160)$ meson at zero temperature by the dotted, dashed, dot-dashed, and solid curves, respectively. The tensor interaction dominates $V_{c\bar{c}}$ at very short distances, but is short range. At short distances, $V_{c\bar{c}}$ increases with increasing distance, while the spin-spin interaction is positive and decreases rapidly. At long distances, $V_{c\bar{c}}$ approaches 0.91 GeV, while the spin-spin interaction almost becomes zero.

The Schrödinger equation with the potential $V_{ab}(\vec{r}_{ab})$ at zero temperature gives meson masses that are close to the experimental masses of π, ρ, K, K^*, J/ψ, χ_c, ψ', $\psi(3770)$, $\psi(4040)$, $\psi(4160)$, $\psi(4415)$, D, D^*, D_s, and D_s^* mesons [21]. The experimental data of S- and P-wave elastic phase shifts for $\pi\pi$ scattering in vacuum [22,23] are reproduced in the Born approximation [24,25]. In the calculations of the meson masses and the phase shifts, the masses of the up quark, down quark, strange quark, and charm quark are kept as 0.32, 0.32, 0.5, and 1.51 GeV, respectively.

In Eqs. (4) and (6), the flavor matrix elements $\varphi^+_{CD\text{flavor}}\varphi_{AB\text{flavor}}$ equal 1. Related to the potential, $\phi^+_{C\text{color}}\phi^+_{D\text{color}}\phi_{A\text{color}}\phi_{B\text{color}}$ is $\frac{1}{3}$, and $\phi^+_{C\text{color}}\phi^+_{D\text{color}}\frac{\vec{\lambda}_a}{2}\cdot\frac{\vec{\lambda}_b}{2}\phi_{A\text{color}}\phi_{B\text{color}}$ are $-\frac{4}{9}$, $-\frac{4}{9}$, $\frac{4}{9}$, $\frac{4}{9}$, $-\frac{4}{9}$, and $-\frac{4}{9}$ for $V_{c\bar{c}}$, $V_{\bar{q}_2 q_1}$, V_{cq_1}, $V_{\bar{q}_2\bar{c}}$, $V_{q_1\bar{c}}$, and $V_{\bar{q}_2 c}$, respectively.

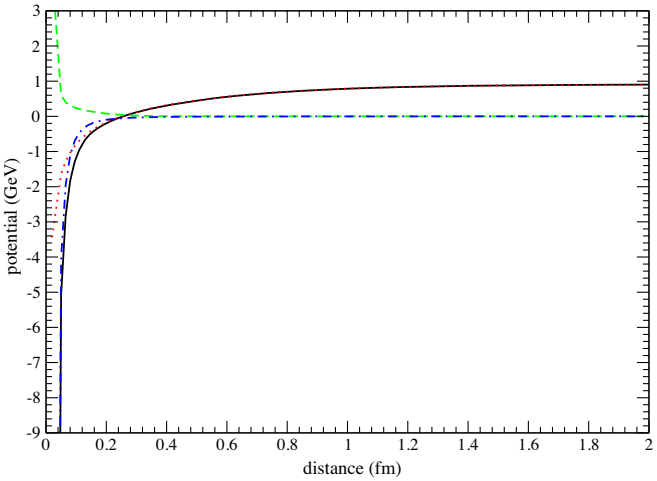

FIG. 3. Potentials as functions of the distance between the quark and the antiquark. The spin-independent potential, spin-spin interaction, and tensor interaction are shown by the dotted, dashed, and dot-dashed curves, respectively. The solid curve indicates the sum of the spin-independent potential, spin-spin interaction, and tensor interaction.

From m_A, m_B, m_C, and m_D, which are the masses of mesons A, B, C, and D, $\vec{P}$ and $\vec{P}'$ are given by

$$\vec{P}^2(\sqrt{s}) = \frac{1}{4s}[(s - m_A^2 - m_B^2)^2 - 4m_A^2 m_B^2], \tag{9}$$

$$\vec{P}'^2(\sqrt{s}) = \frac{1}{4s}[(s - m_C^2 - m_D^2)^2 - 4m_C^2 m_D^2], \tag{10}$$

where the Mandelstam variable $s = (P_A + P_B)^2$ is defined from the four-momenta of mesons A and B, P_A and P_B. Let J_{Az} (J_{Bz}, J_{Cz}, J_{Dz}) denote the magnetic projection quantum number of the total angular momentum J_A (J_B, J_C, J_D) of meson A (B, C, D). When the transition amplitude for scattering in the prior form equals the one for scattering in the post form, i.e., no post-prior discrepancy exists, the unpolarized cross section may be calculated from $\mathcal{M}_{\rm fi}^{\rm prior}$,

$$\sigma_{\rm unpol}^{\rm prior}(\sqrt{s}, T) = \frac{1}{(2J_A+1)(2J_B+1)} \frac{1}{32\pi s} \frac{|\vec{P}'(\sqrt{s})|}{|\vec{P}(\sqrt{s})|} \times \int_0^\pi d\theta \sum_{J_{Az}J_{Bz}J_{Cz}J_{Dz}} |\mathcal{M}_{\rm fi}^{\rm prior}|^2 \sin\theta, \tag{11}$$

or from $\mathcal{M}_{\rm fi}^{\rm post}$,

$$\sigma_{\rm unpol}^{\rm post}(\sqrt{s}, T) = \frac{1}{(2J_A+1)(2J_B+1)} \frac{1}{32\pi s} \frac{|\vec{P}'(\sqrt{s})|}{|\vec{P}(\sqrt{s})|} \times \int_0^\pi d\theta \sum_{J_{Az}J_{Bz}J_{Cz}J_{Dz}} |\mathcal{M}_{\rm fi}^{\rm post}|^2 \sin\theta, \tag{12}$$

where θ is the angle between $\vec{P}$ and $\vec{P}'$. When the transition amplitude for scattering in the prior form does not equal the one for scattering in the post form, i.e., the post-prior discrepancy occurs, we treat $\mathcal{M}_{\rm fi}^{\rm prior}$ and $\mathcal{M}_{\rm fi}^{\rm post}$ on a completely equal footing, and the unpolarized cross section for $A + B \to C + D$ is

$$\begin{aligned}\sigma^{\rm unpol}(\sqrt{s}, T) &= \frac{1}{2}[\sigma_{\rm unpol}^{\rm prior}(\sqrt{s}, T) + \sigma_{\rm unpol}^{\rm post}(\sqrt{s}, T)] \\ &= \frac{1}{(2J_A+1)(2J_B+1)} \frac{1}{64\pi s} \frac{|\vec{P}'(\sqrt{s})|}{|\vec{P}(\sqrt{s})|} \\ &\quad \times \int_0^\pi d\theta \sum_{J_{Az}J_{Bz}J_{Cz}J_{Dz}} (|\mathcal{M}_{\rm fi}^{\rm prior}|^2 + |\mathcal{M}_{\rm fi}^{\rm post}|^2) \sin\theta.\end{aligned} \tag{13}$$

In fact, this equation gives $\sigma^{\rm unpol} = \sigma_{\rm unpol}^{\rm prior} = \sigma_{\rm unpol}^{\rm post}$ when $\mathcal{M}_{\rm fi}^{\rm prior} = \mathcal{M}_{\rm fi}^{\rm post}$. Hence, Eq. (13) is used to calculate the unpolarized cross section. The cross section depends on temperature and the total energy of the two initial mesons in the center-of-mass frame.

III. MASTER RATE EQUATIONS

We use the notation $D = \begin{pmatrix} D^+ \\ D^0 \end{pmatrix}$ and $\bar{D} = \begin{pmatrix} \bar{D}^0 \\ D^- \end{pmatrix}$ for the pseudoscalar isospin doublets as well as $D^* = \begin{pmatrix} D^{*+} \\ D^{*0} \end{pmatrix}$ and $\bar{D}^* = \begin{pmatrix} \bar{D}^{*0} \\ D^{*-} \end{pmatrix}$ for the vector isospin doublets. In hadronic matter number densities for $\psi(4040)$, $\psi(4160)$, and $\psi(4415)$ mesons change with respect to time and space according to the following rate equations:

$$\partial_\mu(n_R u^\mu) = \Theta_R, \tag{14}$$

where μ is the space-time index, and $u^\mu = (u^0, \vec{u})$ is the four-velocity of a fluid element in hadronic matter. $n_{\psi(4040)}$, $n_{\psi(4160)}$, and $n_{\psi(4415)}$ are the number densities of $\psi(4040)$, $\psi(4160)$, and $\psi(4415)$, if R stands for $\psi(4040)$, $\psi(4160)$, and $\psi(4415)$, respectively. In the present work, we take into account only these reactions,

$$\begin{aligned} D\bar{D} &\to \rho R; \qquad D\bar{D}^* \to \pi R, \rho R; \\ D^*\bar{D} &\to \pi R, \rho R; \quad D^*\bar{D}^* \to \pi R, \rho R, \end{aligned}$$

where light mesons in these final states are limited to pions and ρ mesons. The source terms are given by

$$\begin{aligned}\Theta_R = &\langle\sigma_{D\bar{D}\to\rho R} v_{D\bar{D}}\rangle n_D n_{\bar{D}} + \langle\sigma_{D\bar{D}^*\to\pi R} v_{D\bar{D}^*}\rangle n_D n_{\bar{D}^*} \\ &+ \langle\sigma_{D^*\bar{D}\to\pi R} v_{D^*\bar{D}}\rangle n_{D^*} n_{\bar{D}} + \langle\sigma_{D\bar{D}^*\to\rho R} v_{D\bar{D}^*}\rangle n_D n_{\bar{D}^*} \\ &+ \langle\sigma_{D^*\bar{D}\to\rho R} v_{D^*\bar{D}}\rangle n_{D^*} n_{\bar{D}} + \langle\sigma_{D^*\bar{D}^*\to\pi R} v_{D^*\bar{D}^*}\rangle n_{D^*} n_{\bar{D}^*} \\ &+ \langle\sigma_{D^*\bar{D}^*\to\rho R} v_{D^*\bar{D}^*}\rangle n_{D^*} n_{\bar{D}^*}.\end{aligned} \tag{15}$$

The thermal-averaged cross section with the relative velocity of two initial mesons is defined as

$$\langle\sigma_{ij\to i'j'} v_{ij}\rangle = \frac{\int \frac{d^3k_i}{(2\pi)^3} f_i(k_i) \frac{d^3k_j}{(2\pi)^3} f_j(k_j) \sigma_{ij\to i'j'}(\sqrt{s}, T) v_{ij}}{\int \frac{d^3k_i}{(2\pi)^3} f_i(k_i) \int \frac{d^3k_j}{(2\pi)^3} f_j(k_j)}, \tag{16}$$

where $f_i(k_i)$ and $f_j(k_j)$ are the momentum distribution functions of mesons i and j with the four-momenta k_i and k_j in the rest frame of hadronic matter, respectively. $\sigma_{ij\to i'j'}(\sqrt{s})$ is the isospin-averaged unpolarized cross section for $ij \to i'j'$ and is obtained from the unpolarized cross section given in Eq. (13) according to formulas given in the Appendix. v_{ij} is the relative velocity of meson i with mass m_i and meson j with mass m_j,

$$v_{ij} = \frac{\sqrt{(k_i \cdot k_j)^2 - m_i^2 m_j^2}}{k_i^0 k_j^0}. \tag{17}$$

The momentum distribution functions in Eq. (16) with the subscripts suppressed are expressed as

$$f(k) = \frac{1 + \sum_{l=1}^{\infty} c_l (k \cdot u)^l}{e^{k\cdot u/T} - 1}, \tag{18}$$

where the term $\sum_{l=1}^{\infty} c_l (k \cdot u)^l$ indicates deviation from equilibrium.

Denote by $\vec{k}'$ the meson momentum in the local reference frame established on the fluid element, and the meson energy is $k'^0 = k \cdot u$. The number density of the charmed meson is

$$\begin{aligned} n &= g \int \frac{d^3k}{(2\pi)^3} f(k) \\ &= \frac{u^0 g}{2\pi^2} \int_0^\infty d|\vec{k}'| \frac{\vec{k}'^2 \left[1 + \sum_{l=1}^{\infty} c_l \left(\sqrt{\vec{k}'^2 + m^2}\right)^l\right]}{e^{\sqrt{\vec{k}'^2+m^2}/T} - 1}, \end{aligned} \tag{19}$$

where g is the degeneracy factor, and m is the mass of the charmed meson. The thermal-averaged cross section is

$$\langle \sigma_{ij\to i'j'} v_{ij} \rangle = \frac{\int d^3k_i' d^3k_j' f_i'(k_i') f_j'(k_j') \sigma_{ij\to i'j'}(\sqrt{s}, T) v_{ij}'}{(u^0)^2 \int d^3k_i' d^3k_j' f_i'(k_i') f_j'(k_j')}, \tag{20}$$

with

$$f_i'(k_i') = \frac{1 + \sum_{l=1}^{\infty} c_l (k_i'^0)^l}{e^{k_i'^0/T} - 1}, \tag{21}$$

$$f_j'(k_j') = \frac{1 + \sum_{l=1}^{\infty} c_l (k_j'^0)^l}{e^{k_j'^0/T} - 1}, \tag{22}$$

$$v_{ij}' = \frac{\sqrt{(k_i' \cdot k_j')^2 - m_i^2 m_j^2}}{k_i'^0 k_j'^0}. \tag{23}$$

The present work relates to hadronic matter produced in central nucleus-nucleus collisions. Denote by (x, y, z) the Cartesian coordinates of the fluid element (the origin of the local reference frame) in hadronic matter. The four-velocity of the fluid element takes the form $u^\mu = \gamma(\frac{t}{\tau}, v_r \cos\phi, v_r \sin\phi, \frac{z}{\tau})$ where t is the time, $\tau = \sqrt{t^2 - z^2}$ is the proper time, v_r is the transverse velocity, and $\gamma = 1/\sqrt{1 - v_r^2}$ is the Lorentz factor. The z axis in the rest frame of hadronic matter is set along the moving direction of a nucleus and goes through the nuclear center. In central collisions, hadronic matter has only radial flow and longitudinal flow. In terms of the proper time and the cylindrical polar coordinates (r, ϕ, z), the left-hand side in Eq. (14) becomes

$$\partial_\mu (n_R u^\mu) = \gamma \frac{\partial n_R}{\partial \tau} + n_R \left(\frac{\partial \gamma}{\partial \tau} + \frac{\gamma}{\tau}\right) + \frac{1}{r}\frac{\partial}{\partial r}(r n_R \gamma v_r). \tag{24}$$

Hadronic matter possesses cylindrical symmetry. Equation (24) is then reduced to

$$\begin{aligned} \partial_\mu (n_R u^\mu) = {} & \gamma \frac{\partial n_R}{\partial \tau} + \gamma v_r \frac{\partial n_R}{\partial r} + n_R \gamma^3 v_r \frac{\partial v_r}{\partial \tau} \\ & + n_R \gamma^3 \frac{\partial v_r}{\partial r} + \frac{n_R \gamma}{\tau} + \frac{n_R \gamma v_r}{r}. \end{aligned} \tag{25}$$

Combining Eqs. (14), (15), and (25), we get

$$\begin{aligned} & \gamma \frac{\partial n_R}{\partial \tau} + \gamma v_r \frac{\partial n_R}{\partial r} + n_R \gamma^3 v_r \frac{\partial v_r}{\partial \tau} + n_R \gamma^3 \frac{\partial v_r}{\partial r} + \frac{n_R \gamma}{\tau} + \frac{n_R \gamma v_r}{r} \\ & = \langle \sigma_{D\bar{D}\to\rho R} v_{D\bar{D}} \rangle n_D n_{\bar{D}} + \langle \sigma_{D\bar{D}^*\to\pi R} v_{D\bar{D}^*} \rangle n_D n_{\bar{D}^*} \\ & \quad + \langle \sigma_{D^*\bar{D}\to\pi R} v_{D^*\bar{D}} \rangle n_{D^*} n_{\bar{D}} + \langle \sigma_{D\bar{D}^*\to\rho R} v_{D\bar{D}^*} \rangle n_D n_{\bar{D}^*} \\ & \quad + \langle \sigma_{D^*\bar{D}\to\rho R} v_{D^*\bar{D}} \rangle n_{D^*} n_{\bar{D}} + \langle \sigma_{D^*\bar{D}^*\to\pi R} v_{D^*\bar{D}^*} \rangle n_{D^*} n_{\bar{D}^*} \\ & \quad + \langle \sigma_{D^*\bar{D}^*\to\rho R} v_{D^*\bar{D}^*} \rangle n_{D^*} n_{\bar{D}^*}. \end{aligned} \tag{26}$$

The temperature and the transverse velocity involved in Eq. (26) are given by the relativistic hydrodynamic equation,

$$\partial_\mu T^{\mu\nu} = 0, \tag{27}$$

where $T^{\mu\nu}$ is the energy-momentum tensor,

$$\begin{aligned} T^{\mu\nu} = {} & (\epsilon + P) u^\mu u^\nu - P g^{\mu\nu} \\ & + \eta \left[\nabla^\mu u^\nu + \nabla^\nu u^\mu - \frac{2}{3}(g^{\mu\nu} - u^\mu u^\nu) \nabla \cdot u\right], \end{aligned} \tag{28}$$

where ϵ is the energy density, P is the pressure, $g^{\mu\nu}$ is the metric, η is the shear viscosity, and $\nabla^\mu = \partial^\mu - u^\mu u \cdot \partial$. A parametrization of the shear viscosity is given in Ref. [26].

IV. NUMERICAL RESULTS AND DISCUSSIONS

Hadronic matter created in ultrarelativistic heavy-ion collisions changes during expansion. Numerical cross sections obtained from Eq. (13) show remarkable temperature dependence. $\psi(4040)$, $\psi(4160)$, and $\psi(4415)$ mesons produced in hadronic matter are appropriate to measurements.

A. Cross sections

The potential given in Eq. (7) at large distances decreases with increasing temperature, i.e., confinement becomes weaker and weaker. We solve the Schrödinger equation with the potential to obtain meson masses and mesonic

quark-antiquark relative-motion wave functions in coordinate space. The wave functions depend on temperature, and give meson radii which increase with increasing temperature. From the Fourier transform, we get the potential and the wave functions in momentum space, which are used in Eqs. (4) and (6). We calculate transition amplitudes in the prior form and in the post form, which lead to unpolarized cross sections. The unpolarized cross sections depend on temperature and are plotted in Figs. 4–18 for the 15 reactions,

$$
\begin{aligned}
&D\bar{D} \to \rho\psi(4040), \quad D\bar{D} \to \rho\psi(4160), \quad D\bar{D} \to \rho\psi(4415),\\
&D\bar{D}^* \to \pi\psi(4040), \quad D\bar{D}^* \to \pi\psi(4160), \quad D\bar{D}^* \to \pi\psi(4415),\\
&D\bar{D}^* \to \rho\psi(4040), \quad D\bar{D}^* \to \rho\psi(4160), \quad D\bar{D}^* \to \rho\psi(4415),\\
&D^*\bar{D}^* \to \pi\psi(4040), \quad D^*\bar{D}^* \to \pi\psi(4160), \quad D^*\bar{D}^* \to \pi\psi(4415),\\
&D^*\bar{D}^* \to \rho\psi(4040), \quad D^*\bar{D}^* \to \rho\psi(4160), \quad D^*\bar{D}^* \to \rho\psi(4415).
\end{aligned}
$$

The cross sections for $D^*\bar{D}$ reactions are identical to those for $D\bar{D}^*$ reactions. Since the isospin quantum numbers of $\psi(4040)$, $\psi(4160)$, and $\psi(4415)$ are zero, the total isospin of final mesons is that of the pion or the ρ meson.

The reactions that have ρ mesons in the final states are endothermic reactions. The cross section for every endothermic reaction at a given temperature has a maximum; i.e., every cross section curve has at least one peak. Weakening confinement leads to decreasing cross section with increasing temperature. However, increase of initial-meson radii cause an increase of cross sections. The two factors generate variation of the peak cross section with increasing temperature. At zero temperature the peak cross sections of $D\bar{D} \to \rho\psi(4160)$ $[D\bar{D}^* \to \rho\psi(4160),\ D^*\bar{D}^* \to \rho\psi(4160)]$ and $D\bar{D} \to \rho\psi(4415)$ $[D\bar{D}^* \to \rho\psi(4415),\ D^*\bar{D}^* \to \rho\psi(4415)]$ are similar, but smaller than that of $D\bar{D} \to \rho\psi(4040)$ $[D\bar{D}^* \to \rho\psi(4040),\ D^*\bar{D}^* \to \rho\psi(4040)]$. At any of the five temperatures $T/T_c = 0.65$, 0.75, 0.85, 0.9, or 0.95, the peak cross section of $D\bar{D} \to \rho\psi(4040)$ $[D\bar{D}^* \to \rho\psi(4040),\ D^*\bar{D}^* \to \rho\psi(4040)]$ is similar to or larger than the one of $D\bar{D} \to \rho\psi(4415)$ $[D\bar{D}^* \to \rho\psi(4415),\ D^*\bar{D}^* \to \rho\psi(4415)]$, and the one of $D\bar{D} \to \rho\psi(4160)$ $[D\bar{D}^* \to \rho\psi(4160), D^*\bar{D}^* \to \rho\psi(4160)]$ is generally much smaller than the latter.

The reactions that produce pions are endothermic at $T = 0$ and exothermic at $T/T_c = 0.65$, 0.75, 0.85, 0.9, and 0.95. For the endothermic reactions, the peak cross section of $D\bar{D}^* \to \pi\psi(4040)$ is larger than the one of $D\bar{D}^* \to \pi\psi(4160)$, which is larger than that of $D\bar{D}^* \to \pi\psi(4415)$. Away from threshold energies, every cross section curve of the exothermic reactions has one or two maxima. The peak cross section of producing $\psi(4040)$ is largest and the one of producing $\psi(4160)$ is smallest among the reactions $D\bar{D}^* \to \pi\psi(4040)$, $D\bar{D}^* \to \pi\psi(4160)$, and $D\bar{D}^* \to \pi\psi(4415)$. A similar case holds true for $D^*\bar{D}^* \to \pi\psi(4040)$, $D^*\bar{D}^* \to \pi\psi(4160)$, and $D^*\bar{D}^* \to \pi\psi(4415)$.

Numerical cross sections plotted in Figs. 4–18 are used in the master rate equations. For convenience, they are parametrized as

$$
\begin{aligned}
\sigma^{\rm unpol}(\sqrt{s},T) = {} & a_1\left(\frac{\sqrt{s}-\sqrt{s_0}}{b_1}\right)^{c_1}\exp\left[c_1\left(1-\frac{\sqrt{s}-\sqrt{s_0}}{b_1}\right)\right]\\
& + a_2\left(\frac{\sqrt{s}-\sqrt{s_0}}{b_2}\right)^{c_2}\exp\left[c_2\left(1-\frac{\sqrt{s}-\sqrt{s_0}}{b_2}\right)\right],
\end{aligned}
\tag{29}
$$

for endothermic reactions and

$$
\sigma^{\rm unpol}(\sqrt{s},T) = \frac{\vec{P'}^2}{\vec{P}^2}\left\{a_1\left(\frac{\sqrt{s}-\sqrt{s_0}}{b_1}\right)^{c_1}\exp\left[c_1\left(1-\frac{\sqrt{s}-\sqrt{s_0}}{b_1}\right)\right] + a_2\left(\frac{\sqrt{s}-\sqrt{s_0}}{b_2}\right)^{c_2}\exp\left[c_2\left(1-\frac{\sqrt{s}-\sqrt{s_0}}{b_2}\right)\right]\right\}, \tag{30}
$$

for exothermic reactions. $\sqrt{s_0}$ is the threshold energy, which equals the sum of the masses of the two initial (final) mesons for the exothermic (endothermic) reaction. The values of the parameters a_1, b_1, c_1, a_2, b_2, and c_2 are listed in Tables I–V, where d_0 is the separation between the peak's location on the $\sqrt{s}$ axis and the threshold energy, and $\sqrt{s_z}$ is the square root of the Mandelstam variable at which the cross section is 1/100 of the peak cross section. The temperature-dependent charmonium masses obtained from the Schrödinger equation are parametrized as

$$
m_{\psi(4040)} = 3.59\left[1-\left(\frac{T}{1.26T_c}\right)^{3.16}\right]^{0.35}, \tag{31}
$$

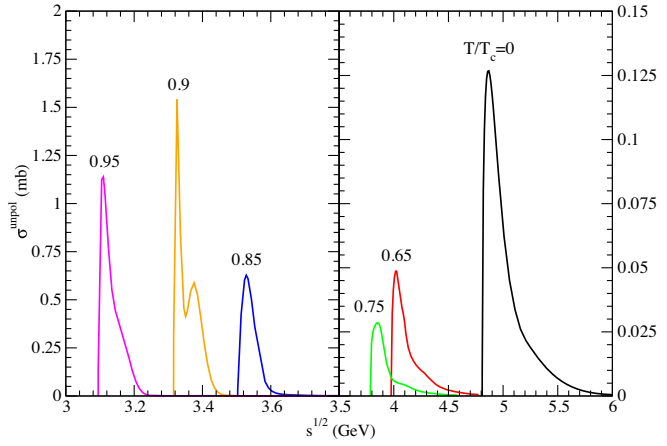

FIG. 4. Cross sections for $D\bar{D} \to \rho\psi(4040)$ at various temperatures.

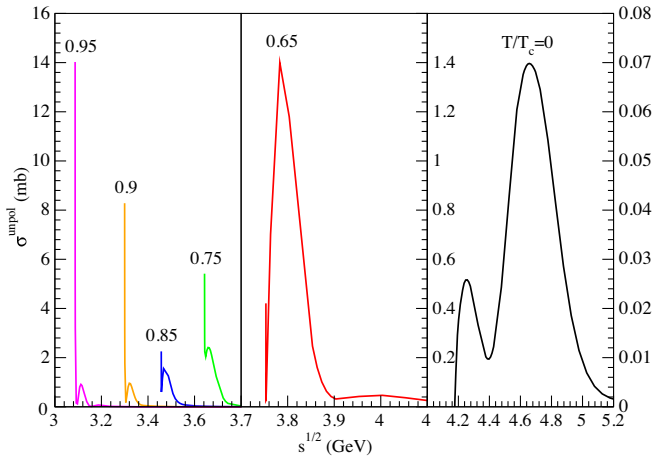

FIG. 7. Cross sections for $D\bar{D}^* \to \pi\psi(4040)$ at various temperatures.

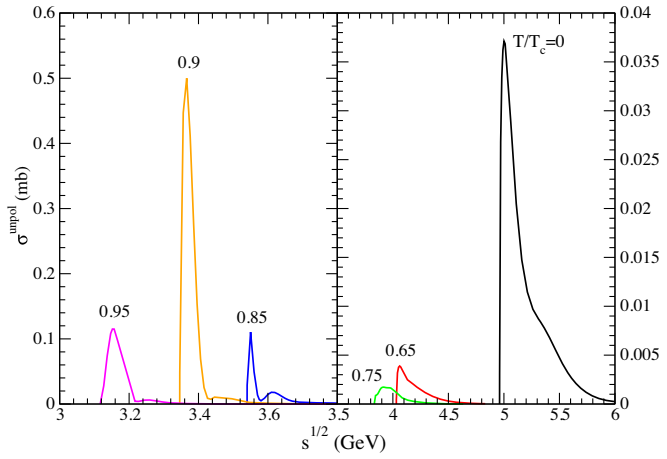

FIG. 5. Cross sections for $D\bar{D} \to \rho\psi(4160)$ at various temperatures.

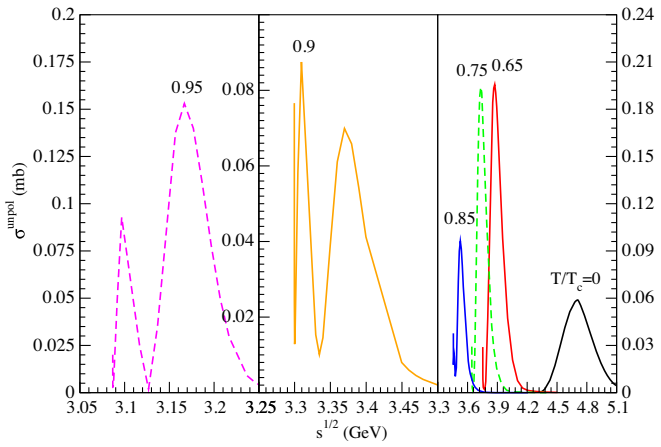

FIG. 8. Cross sections for $D\bar{D}^* \to \pi\psi(4160)$ at various temperatures.

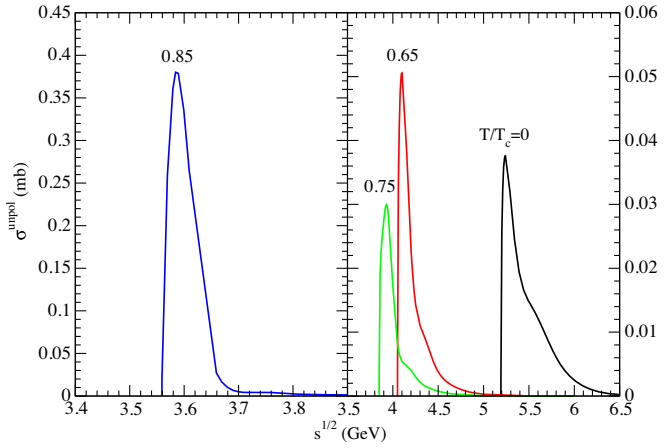

FIG. 6. Cross sections for $D\bar{D} \to \rho\psi(4415)$ at various temperatures.

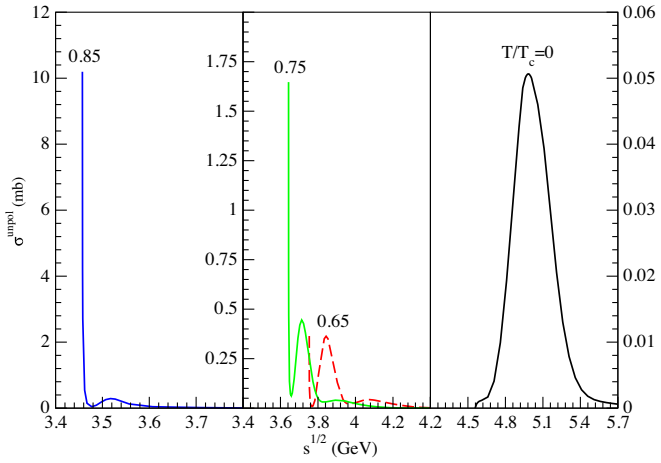

FIG. 9. Cross sections for $D\bar{D}^* \to \pi\psi(4415)$ at various temperatures.

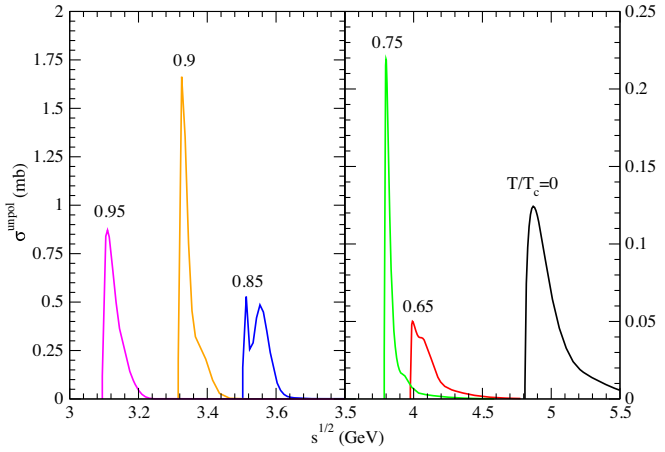

FIG. 10. Cross sections for $D\bar{D}^* \to \rho\psi(4040)$ at various temperatures.

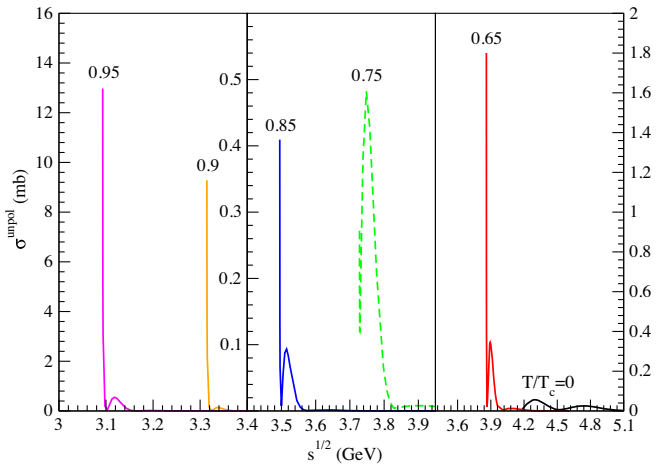

FIG. 13. Cross sections for $D^*\bar{D}^* \to \pi\psi(4040)$ at various temperatures.

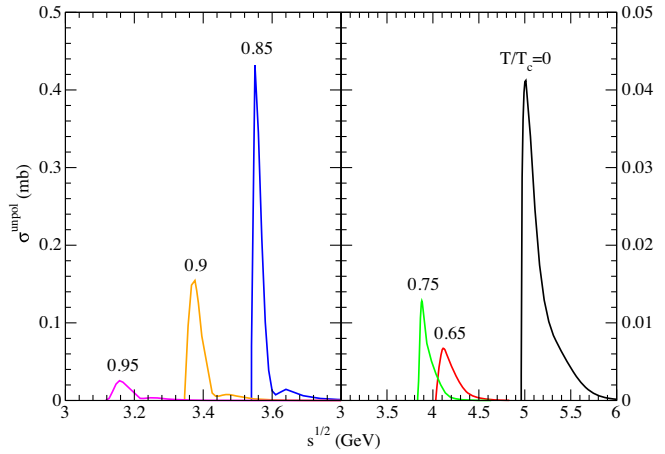

FIG. 11. Cross sections for $D\bar{D}^* \to \rho\psi(4160)$ at various temperatures.

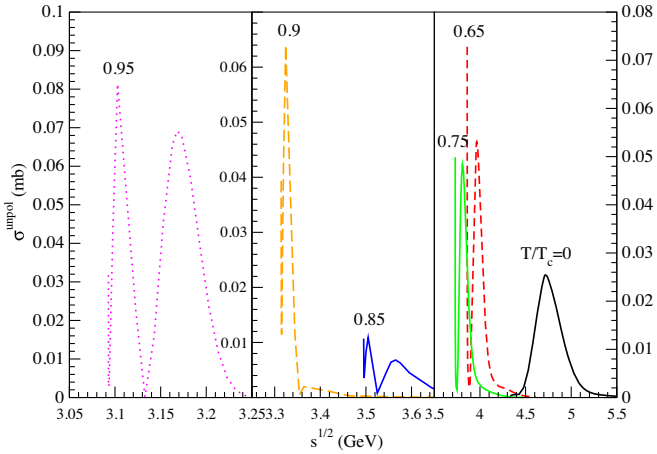

FIG. 14. Cross sections for $D^*\bar{D}^* \to \pi\psi(4160)$ at various temperatures.

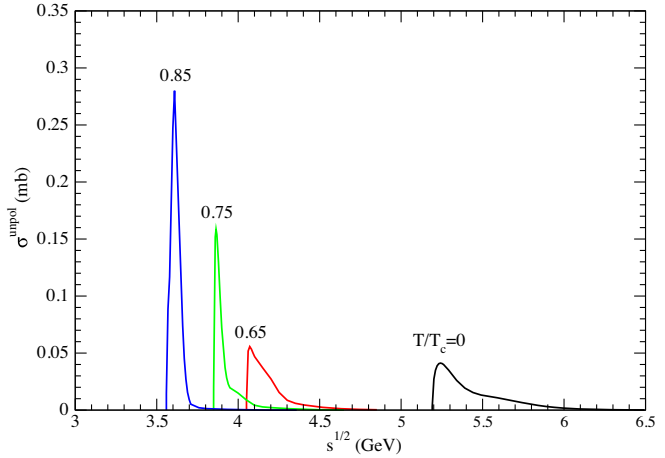

FIG. 12. Cross sections for $D\bar{D}^* \to \rho\psi(4415)$ at various temperatures.

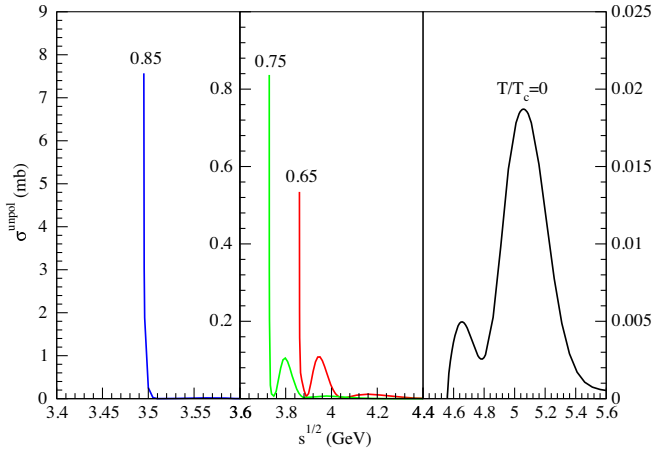

FIG. 15. Cross sections for $D^*\bar{D}^* \to \pi\psi(4415)$ at various temperatures.

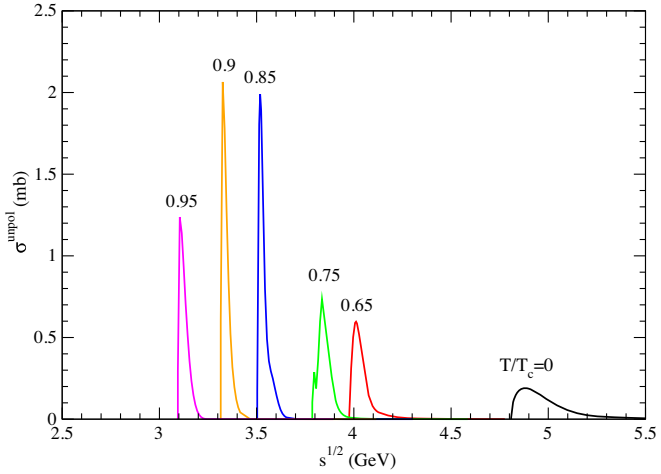

FIG. 16. Cross sections for $D^*\bar{D}^* \to \rho\psi(4040)$ at various temperatures.

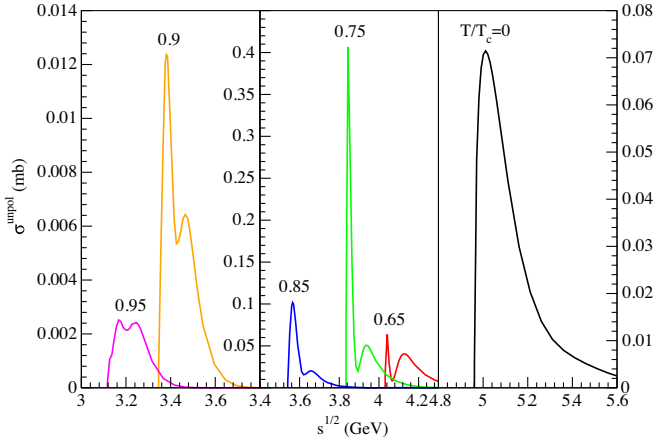

FIG. 17. Cross sections for $D^*\bar{D}^* \to \rho\psi(4160)$ at various temperatures.

$$m_{\psi(4160)} = 3.64\left[1-\left(\frac{T}{1.34T_c}\right)^{3.52}\right]^{0.54}, \tag{32}$$

$$m_{\psi(4415)} = 3.74\left[1-\left(\frac{T}{1.21T_c}\right)^{2.36}\right]^{0.25}. \tag{33}$$

In hadronic matter where the temperature is constrained by $0.6T_c \le T < T_c$, the masses of $\psi(4040)$, $\psi(4160)$, and $\psi(4415)$ are smaller than the sum of two open-charm mesons. Therefore, the production of the three charmonia from fusion of two open-charm mesons is not allowed [17].

The transition amplitudes for scattering in the prior form and in the post form include the Fourier transform of the coordinate-space potential given in Eq. (7),

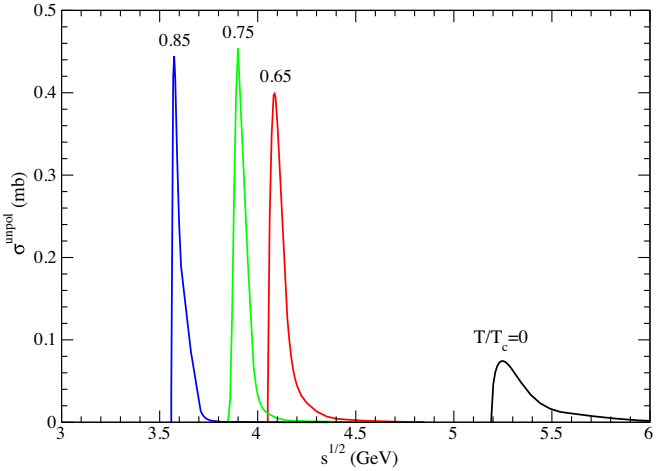

FIG. 18. Cross sections for $D^*\bar{D}^* \to \rho\psi(4415)$ at various temperatures.

$$\begin{aligned}
V_{ab}(\vec{Q}) = &-\frac{\vec{\lambda}_a}{2}\cdot\frac{\vec{\lambda}_b}{2}\xi_1\left[1.3-\left(\frac{T}{T_c}\right)^4\right]\left[(2\pi)^3\delta^3(\vec{Q})-\frac{8\pi}{Q}\int_0^\infty dr\frac{r\sin(Qr)}{\exp(2\xi_2 r)+1}\right]\\
&+\frac{\vec{\lambda}_a}{2}\cdot\frac{\vec{\lambda}_b}{2}64\pi\xi_3\int_0^\infty dq\frac{\rho(q^2)-\frac{K}{q^2}}{(\xi_3^2+Q^2+q^2)^2-4Q^2q^2}\\
&-\frac{\vec{\lambda}_a}{2}\cdot\frac{\vec{\lambda}_b}{2}\frac{16\pi^2}{25}\exp\left(-\frac{Q^2}{4d^2}\right)\frac{\vec{s}_a\cdot\vec{s}_b}{m_a m_b}+\frac{\vec{\lambda}_a}{2}\cdot\frac{\vec{\lambda}_b}{2}\frac{16\pi^2\lambda}{25Q}\int_0^\infty dx\frac{d^2v(x)}{dx^2}\sin\left(\frac{Q}{\lambda}x\right)\frac{\vec{s}_a\cdot\vec{s}_b}{m_a m_b}\\
&-\frac{\vec{\lambda}_a}{2}\cdot\frac{\vec{\lambda}_b}{2}\frac{24\pi^2\lambda}{25Q}\int_0^\infty dx\frac{1}{x^2}\left[v(x)-x\frac{dv(x)}{dx}+\frac{x^2}{3}\frac{d^2v(x)}{dx^2}\right]\\
&\times\left[\left(1-\frac{3\lambda^2}{Q^2x^2}\right)\sin\left(\frac{Q}{\lambda}x\right)+\frac{3\lambda}{Qx}\cos\left(\frac{Q}{\lambda}x\right)\right]\frac{3s_{az}s_{bz}-\vec{s}_a\cdot\vec{s}_b}{m_a m_b},
\end{aligned} \tag{34}$$

where $\vec{Q}$ is the momentum attached to the dot-dashed lines in Figs. 1 and 2, $K = 3/16\pi^2\alpha'$, $\rho(q^2)$ is the physical running coupling constant [18], and s_{az} (s_{bz}) is the magnetic projection quantum number of $\vec{s}_a$ ($\vec{s}_b$). The expressions of $\mathcal{M}_{\rm fi}^{\rm prior}$ and $\mathcal{M}_{\rm fi}^{\rm post}$ with this momentum-space potential involve seven-dimensional integrals. Because of the two sines and the cosine in

TABLE I. Values of the parameters in Eq. (29) for $D\bar{D} \to \rho\psi(4040)$, $\rho\psi(4160)$, and $\rho\psi(4415)$. a_1 and a_2 are in units of millibarns; b_1, b_2, d_0, and $\sqrt{s_z}$ are in units of GeV; c_1 and c_2 are dimensionless.

Reaction	T/T_c	a_1	b_1	c_1	a_2	b_2	c_2	d_0	$\sqrt{s_z}$
$D\bar{D} \to \rho\psi(4040)$	0	0.08	0.05	0.69	0.05	0.07	0.37	0.06	5.82
	0.65	0.04	0.04	0.88	0.01	0.09	0.18	0.045	4.79
	0.75	0.023	0.03	0.44	0.01	0.08	2.62	0.07	4.59
	0.85	0.45	0.03	2.59	0.28	0.01	0.62	0.025	3.65
	0.9	0.53	0.063	10.09	1.57	0.006	0.54	0.06	3.45
	0.95	0.76	0.01	0.85	0.42	0.02	0.32	0.015	3.23
$D\bar{D} \to \rho\psi(4160)$	0	0.03	0.04	0.67	0.01	0.11	0.25	0.04	5.93
	0.65	0.0028	0.05	0.36	0.0013	0.02	1.29	0.03	4.8
	0.75	0.0018	0.1	1.69	0.0007	0.007	0.5	0.08	4.54
	0.85	0.08	0.01	4.45	0.03	0.01	0.01	0.01	3.81
	0.9	0.33	0.02	2.36	0.22	0.01	0.43	0.02	3.52
	0.95	0.1	0.037	4	0.02	0.02	0.9	0.035	3.35
$D\bar{D} \to \rho\psi(4415)$	0	0.04	0.05	0.52	0.01	0.4	7.25	0.05	6.39
	0.65	0.03	0.04	0.86	0.02	0.05	0.35	0.05	4.89
	0.75	0.024	0.04	0.44	0.011	0.09	7.61	0.08	4.7
	0.85	0.3	0.03	2	0.13	0.01	0.52	0.025	3.77

TABLE II. Values of the parameters in Eqs. (29) and (30) for $D\bar{D}^* \to \pi\psi(4040)$, $\pi\psi(4160)$, and $\pi\psi(4415)$. a_1 and a_2 are in units of millibarns; b_1, b_2, d_0, and $\sqrt{s_z}$ are in units of GeV; c_1 and c_2 are dimensionless.

Reaction	T/T_c	a_1	b_1	c_1	a_2	b_2	c_2	d_0	$\sqrt{s_z}$
$D\bar{D}^* \to \pi\psi(4040)$	0	0.08	0.49	16.02	0.022	0.061	0.61	0.48	5.37
	0.65	1.15	0.04	2.81	0.14	0.08	1.31	0.05	4.22
	0.75	1.27	0.032	2.32	0.3	0.026	0.64	0.03	4.03
	0.85	0.96	0.026	1.97	0.07	0.054	0.59	0.03	3.75
	0.9	1.09	0.028	4	0.11	0.001	0.6	0.025	3.54
	0.95	3.42	0.029	6.73	0.81	0.001	0.62	0.03	3.28
$D\bar{D}^* \to \pi\psi(4160)$	0	0.048	0.35	3.65	0.003	0.5	0.62	0.38	5.39
	0.65	0.52	0.123	6.38	0.0014	0.01	0.55	0.12	4.19
	0.75	0.43	0.097	5.87	0.0008	0.006	0.53	0.1	3.99
	0.85	0.2	0.086	8.26	0.012	0.029	0.93	0.08	3.74
	0.9	0.146	0.08	4.16	0.065	0.015	2	0.07	3.54
	0.95	0.83	0.077	7.54	0.45	0.016	2.44	0.08	3.27
$D\bar{D}^* \to \pi\psi(4415)$	0	0.045	0.43	7.82	0.002	0.29	0.51	0.43	5.74
	0.65	0.91	0.091	5.96	0.014	0.004	0.45	0.09	4.34
	0.75	0.9	0.074	5.1	0.046	0.006	0.42	0.08	4.15
	0.85	0.61	0.065	6.34	0.232	0.0024	0.49	0.07	3.85

the fourth and fifth terms, in a short computational time to carry out integration at a given temperature and a given value of $\sqrt{s}$ is impossible. In order to reduce the computational time, the two integrals in the fourth and fifth terms are parametrized as

$$\int_0^\infty dx \frac{d^2v(x)}{dx^2} \sin\left(\frac{Q}{\lambda}x\right) = (1 - 0.36e^{-0.1Q} - 0.58e^{-0.4Q} - 0.06e^{-0.4Q^2})(-1.7 - 0.0575Q), \tag{35}$$

$$\int_0^\infty dx \frac{1}{x^2}\left[v(x) - x\frac{dv(x)}{dx} + \frac{x^2}{3}\frac{d^2v(x)}{dx^2}\right]\left[\left(1 - \frac{3\lambda^2}{Q^2x^2}\right)\sin\left(\frac{Q}{\lambda}x\right) + \frac{3\lambda}{Qx}\cos\left(\frac{Q}{\lambda}x\right)\right]$$
$$= (1 - 0.59e^{-0.15Q} - 0.31e^{-0.3Q^2} - 0.1e^{-6.71Q^2})(-0.568 - 0.0375Q), \tag{36}$$

TABLE III. The same as Table I except for $D\bar{D}^*$ reactions.

Reaction	T/T_c	a_1	b_1	c_1	a_2	b_2	c_2	d_0	$\sqrt{s_z}$
$D\bar{D}^* \to \rho\psi(4040)$	0	0.08	0.09	0.9	0.06	0.03	0.44	0.06	5.69
	0.65	0.05	0.02	0.42	0.02	0.13	4.62	0.015	4.69
	0.75	0.16	0.01	0.47	0.06	0.02	0.9	0.013	4.14
	0.85	0.48	0.05	5.76	0.8	0.004	0.61	0.05	3.66
	0.9	1.5	0.01	1.04	0.22	0.01	0.08	0.01	3.45
	0.95	0.58	0.01	0.44	0.32	0.02	1.16	0.015	3.22
$D\bar{D}^* \to \rho\psi(4160)$	0	0.03	0.04	0.5	0.01	0.1	0.39	0.05	5.86
	0.65	0.004	0.09	2.54	0.003	0.08	0.52	0.08	4.69
	0.75	0.01	0.05	3.16	0.005	0.39	0.36	0.045	4.3
	0.85	0.39	0.006	0.55	0.14	0.02	3.13	0.01	3.72
	0.9	0.12	0.03	3.58	0.07	0.01	0.7	0.03	3.57
	0.95	0.024	0.041	4.73	0.002	0.02	0.7	0.04	3.4
$D\bar{D}^* \to \rho\psi(4415)$	0	0.027	0.04	0.78	0.017	0.1	0.32	0.05	6.26
	0.65	0.048	0.05	0.66	0.022	0.006	0.45	0.02	4.76
	0.75	0.13	0.01	0.52	0.05	0.03	1.82	0.015	4.27
	0.85	0.26	0.047	3.16	0.19	0.003	1.04	0.05	3.75

TABLE IV. The same as Table II except for $D^*\bar{D}^*$ reactions.

Reaction	T/T_c	a_1	b_1	c_1	a_2	b_2	c_2	d_0	$\sqrt{s_z}$
$D^*\bar{D}^* \to \pi\psi(4040)$	0	0.039	0.12	2.99	0.02	0.07	0.6	0.12	5.31
	0.65	0.18	0.044	4.34	0.006	0.0009	0.63	0.045	4.29
	0.75	0.17	0.03	2.44	0.007	0.03	0.63	0.03	4.07
	0.85	0.0515	0.0251	4.71	0.0021	0.0005	1.03	0.025	3.73
	0.9	0.154	0.0275	12.24	0.13	0.0011	0.69	0.025	3.38
	0.95	1.89	0.0287	8.12	0.68	0.001	0.6	0.03	3.16
$D^*\bar{D}^* \to \pi\psi(4160)$	0	0.024	0.4	7.65	0.0006	0.05	0.52	0.39	5.51
	0.65	0.075	0.116	7.05	0.0009	0.007	0.53	0.11	4.48
	0.75	0.063	0.097	6.06	0.0005	0.005	0.54	0.09	4.26
	0.85	0.0091	0.082	4.81	0.0035	0.014	2.01	0.07	3.93
	0.9	0.048	0.014	3.09	0.004	0.12	0.48	0.01	3.55
	0.95	0.37	0.076	15.79	0.32	0.017	2.42	0.075	3.24
$D^*\bar{D}^* \to \pi\psi(4415)$	0	0.019	0.51	16.47	0.0041	0.086	0.61	0.5	5.88
	0.65	0.16	0.09	12.74	0.0111	0.0076	0.72	0.09	4.4
	0.75	0.108	0.074	6.96	0.0053	0.0023	0.36	0.07	4.19
	0.85	0.095	0.0015	0.57	0.03	0.064	12.41	0.001	3.51

where the unit of Q is fm^{-1}. The momentum-space potential with the two parametrizations causes the post-prior discrepancy. To know the contribution from scattering in the prior form or in the post form to the unpolarized cross section σ^{unpol}, in Fig. 19 we compare the cross sections ($\sigma^{\mathrm{prior}}_{\mathrm{unpol}}$ and $\sigma^{\mathrm{post}}_{\mathrm{unpol}}$) for scattering in the prior form and in the post form with the unpolarized cross section (σ^{unpol}) for the exothermic reaction $D\bar{D}^* \to \pi\psi(4040)$ at $T/T_c = 0.85$ and the endothermic reaction $D\bar{D}^* \to \rho\psi(4040)$. At few energies, for example, $\sqrt{s} = 3.765$ GeV in the right panel, the dotted curves and the dashed curves cross, i.e., $\sigma^{\mathrm{prior}}_{\mathrm{unpol}} = \sigma^{\mathrm{post}}_{\mathrm{unpol}} = \sigma^{\mathrm{unpol}}$, which indicates that scattering in the prior form and in the post form make the same contribution to σ^{unpol}. When $\sqrt{s}$ increases from 3.6 GeV, the dotted curves approach the dashed curves, which means that the post-prior discrepancy becomes smaller and smaller. The threshold energy of $D\bar{D}^* \to \pi\psi(4040)$ at $T/T_c = 0.85$ is 3.45709 GeV. At $\sqrt{s} = 3.4571$ GeV the cross section for scattering in the prior form is 81.7% smaller than σ^{unpol}, while the cross section for scattering in the post form is 81.7% larger than σ^{unpol}. At $\sqrt{s} = 3.47209$ GeV the solid curve exhibits a maximum, and $\sigma^{\mathrm{prior}}_{\mathrm{unpol}}$ ($\sigma^{\mathrm{post}}_{\mathrm{unpol}}$) is 68.7% larger (smaller) than σ^{unpol}. In the right panel, σ^{unpol} for $D\bar{D}^* \to \rho\psi(4040)$ at $\sqrt{s} = 3.51319$ (3.52569, 3.55569) GeV has a maximum (minimum, maximum), and $\sigma^{\mathrm{prior}}_{\mathrm{unpol}}$ and $\sigma^{\mathrm{post}}_{\mathrm{unpol}}$ deviate from σ^{unpol} by 5.6% (87%, 59.7%). Contributions from scattering

TABLE V. The same as Table I except for $D^*\bar{D}^*$ reactions.

Reaction	T/T_c	a_1	b_1	c_1	a_2	b_2	c_2	d_0	$\sqrt{s_z}$
$D^*\bar{D}^* \to \rho\psi(4040)$	0	0.13	0.04	0.5	0.09	0.12	1.47	0.07	5.65
	0.65	0.51	0.04	2.2	0.19	0.01	0.6	0.035	4.28
	0.75	0.78	0.057	5.71	0.36	0.004	0.47	0.05	4
	0.85	1.33	0.01	0.57	0.73	0.02	2.87	0.015	3.64
	0.9	1.69	0.006	0.33	0.61	0.02	1.7	0.01	3.44
	0.95	1.06	0.01	0.36	0.21	0.02	2.06	0.01	3.21
$D^*\bar{D}^* \to \rho\psi(4160)$	0	0.05	0.03	0.47	0.03	0.1	1.02	0.05	5.78
	0.65	0.085	0.0042	0.58	0.04	0.108	4.45	0.01	4.5
	0.75	0.32	0.01	1.76	0.09	0.01	0.04	0.01	4.14
	0.85	0.07	0.03	3.36	0.05	0.01	0.67	0.025	3.84
	0.9	0.008	0.03	6.22	0.0062	0.061	0.421	0.035	3.68
	0.95	0.0017	0.104	2.34	0.0012	0.028	0.396	0.05	3.47
$D^*\bar{D}^* \to \rho\psi(4415)$	0	0.06	0.04	0.5	0.02	0.11	1.03	0.06	6.12
	0.65	0.34	0.04	1.7	0.13	0.009	0.48	0.035	4.41
	0.75	0.48	0.054	3.63	0.01	3.24	0.13	0.05	4.1
	0.85	0.33	0.01	0.64	0.14	0.03	0.84	0.015	3.74

in the prior form and in the post form change with increasing $\sqrt{s}$.

The potential used by Barnes and Swanson in Ref. [16] includes the color Coulomb interaction, the linear confining interaction, and the one-gluon-exchange spin-spin hyperfine interaction. Describing quark-antiquark relative motion in all mesons by a Gaussian wave function, they obtained that the cross section for elastic $\pi\pi$ (KK) scattering for total isospin $I = 2$ ($I = 1$) in the post form equals the one in the prior form. This means that the scattering amplitude in the post form equals the scattering amplitude in the prior form, even though the Gaussian wave function is not the exact quark-antiquark relative-motion wave functions that are solutions of the Schrödinger equation with the potential. Matrix elements of the spin-spin hyperfine interaction in scattering in the prior form are given by Eqs. (71)–(74) in Ref. [16] when the four constituents of scattering mesons have the same mass. However, the four equations are not enough to help us in understanding that the scattering amplitude in the post form equals the one in the prior form. Therefore, in Ref. [27] we present analytic expressions of all matrix elements of the spin-spin interaction in scattering in the post form and in the prior form allowing that the four constituents have different masses and that different Gaussian wave functions are used to describe quark-antiquark relative motion of different mesons. Every matrix element is the product of a flavor matrix element, a color matrix element, a spin matrix element, and a spatial matrix element. The two upper diagrams in Fig. 1 (Fig. 2) are capture diagrams in which the interacting quark-antiquark pair scatter into (come from) the same final (initial) meson. The four lower diagrams in Figs. 1 and 2 are transfer diagrams in which the two interacting quarks or antiquarks scatter into different final mesons. The transfer diagrams in the post and prior forms are identical, and the capture diagrams in the two forms look different. A matrix element is associated with a diagram. When the sum of the two matrix elements corresponding to the capture diagrams in the post form does not equal the sum in the prior form, the post-prior discrepancy occurs. The same flavor matrix element is applied to the eight diagrams in Figs. 1 and 2. The color matrix elements associated with the four capture diagrams are all $-4/9$. For elastic scattering of two pseudoscalar mesons, the spin matrix elements corresponding to the four capture diagrams are the same. Hence, the matrix element of the spin-spin interaction in a (the other) capture diagram in the post form equals the one in a

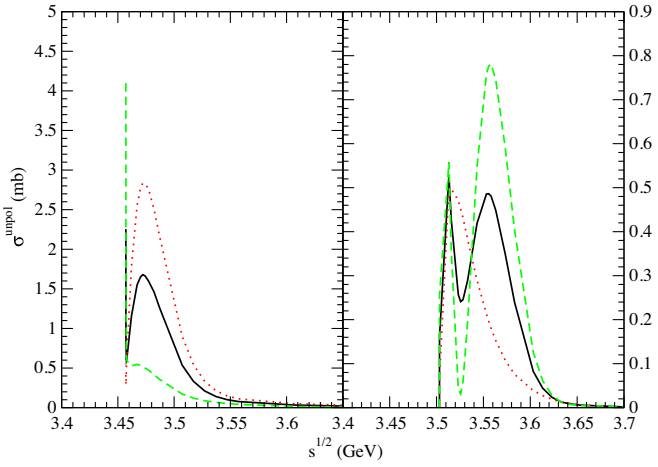

FIG. 19. Cross sections for $D\bar{D}^* \to \pi\psi(4040)$ (left) and for $D\bar{D}^* \to \rho\psi(4040)$ (right) at $T/T_c = 0.85$. $\sigma^{\rm unpol}$, $\sigma^{\rm prior}_{\rm unpol}$, and $\sigma^{\rm post}_{\rm unpol}$ are shown by the solid, dotted, and dashed curves, respectively.

(the other) capture diagram in the prior form, if the Gaussian wave functions of the initial and final mesons are identical and the quarks or the antiquarks of scattering mesons have the same flavor [27]. Numerical calculations show that the matrix element of the central spin-independent potential in the post form equals the one in the prior form [27]. Therefore, the scattering amplitude in the post form equals the scattering amplitude in the prior form, and no post-prior discrepancy happens in elastic scattering of two pseudoscalar mesons [16,27], when the quark-antiquark relative motion of the initial and final mesons are described by the same Gaussian wave function and if the quarks or the antiquarks of scattering mesons have the same flavor. No post-prior discrepancy is also true for elastic scattering between two vector mesons or between a pseudoscalar meson and a vector meson [27].

In Ref. [16] $H_0(A)$, $H_0(B)$, $H_0(C)$, and $H_0(D)$ of mesons A, B, C, and D in the scattering $A+B\to C+D$ individually consist of the kinetic energies of the quark and the antiquark and the potential between the quark and the antiquark. The Schrödinger equation with H_0 provides masses and exact quark-antiquark relative-motion wave functions of the four mesons. The interaction $H_I(A,B)$ between the two constituents of meson A and the two constituents of meson B turns the color-singlet states A and B into color-octet states. During propagation of quarks and antiquarks, quark interchange causes a quark and an antiquark to form the color-singlet state C, as well as the other quark and the other antiquark to form the color-singlet state D. This decomposition of the Hamiltonian of the four constituents $H=H_0(A)+H_0(B)+H_I(A,B)$ reflects the prior form of scattering. Certainly, quark interchange between mesons A and B can take place before the interaction $H_I(C,D)$ between the two constituents of meson C and the two constituents of meson D and breaks up mesons A and B to yield two color-octet states. The interaction $H_I(C,D)$ makes the two color-octet states colorless so that the bound states C and D are formed. Scattering in the post form thus gives rise to this decomposition $H=H_0(C)+H_0(D)+H_I(C,D)$. Therefore, the post-prior discrepancy [originally the $H_I(A,B)$ matrix element does not equal the $H_I(C,D)$ matrix element] is related to the decomposition of the Hamiltonian.

If two or more mesons in elastic meson-meson scattering are described by different Gaussian wave functions, the scattering amplitudes in the post form and in the prior form are not the same, and the post-prior discrepancy takes place [27]. For inelastic scattering of two mesons, the spin matrix elements associated with the four capture diagrams cannot guarantee that the sum of the two matrix elements corresponding to the capture diagrams in the post form equals the sum in the prior form, the scattering amplitudes in the two forms are thus not identical, and the post-prior discrepancy occurs [16]. If the exact mesonic quark-antiquark wave functions are used, no post-prior discrepancy exists. However, the exact wave functions are not amenable to analytic calculations. To get analytic expressions of spatial matrix elements, the sum of several Gaussian wave functions was suggested in Ref. [16] to approach the exact quark-antiquark relative-motion wave functions. The more Gaussian wave functions that are used, the smaller post-prior discrepancy that is observed.

B. Number densities

Since charmed mesons are well measured in Pb-Pb collisions at the LHC, we get their distribution functions $f(k)$ from experimental data. The Cooper-Frye formula [28] is

$$E\frac{d^3N}{d^3k}=\frac{g}{(2\pi)^3}\int_{\sigma_f}f(k)k^\mu d\sigma_\mu, \tag{37}$$

where E, k^μ, and N are the energy, the four-momentum, and the number of the charmed meson, respectively; σ_f is the freeze-out surface with the normal vector $d\sigma_\mu$. With the space-time rapidity $\eta=\frac{1}{2}\ln\frac{t+z}{t-z}$, we get

$$\begin{aligned}\frac{dN}{dk_T}=&\frac{g}{(2\pi)^3}\int_{R_c}^{R_{fz}}\int_0^{2\pi}\int_{-10}^{10}\int_0^{2\pi}\int_{y_{min}}^{y_{max}}\\&\times f(k)[m_T\cosh(y-\eta)-k_Tv_r\cos(\phi-\varphi)]\\&\times k_T\tau r dr d\phi d\eta d\varphi dy,\end{aligned} \tag{38}$$

where y, $\vec{k}_T$, and m_T are the rapidity, transverse momentum, and transverse mass of the charmed meson, respectively; φ is the angle between the transverse momentum and the x axis; R_c and R_{fz} are the radii of hadronic-matter surface at hadronization and at kinetic freeze-out, respectively. In Ref. [29] the D-meson production yields are measured at midrapidity ($|y|<0.5$) as functions of transverse momentum. y_{min} and y_{max} are thus set as -0.5 and 0.5, respectively. Fits to the experimental data of dN/dp_T of prompt D^+, D^0, and D^{*+} mesons at $p_T<8$ GeV/c in central Pb-Pb collisions at $\sqrt{s_{NN}}=5.02$ TeV with $T=0.1686$ GeV give

$$\begin{aligned}&l=11,\quad c_l=6\times10^{-12},\quad \text{for } D^+ \text{ meson};\\&l=9,\quad c_l=3\times10^{-9},\quad \text{for } D^0 \text{ meson};\\&l=14,\quad c_l=5\times10^{-16},\quad \text{for } D^{*+} \text{ meson};\end{aligned}$$

c_l equal zero for other l values. This means that only one term in the sum $\sum_{l=1}^{\infty}c_l(k\cdot u)^l$ is needed for each D meson.

Quark-gluon matter initially produced in Pb-Pb collisions at LHC energies is not a thermal state. Undergoing elastic parton-parton-parton scattering and parton-parton scattering, quark-gluon matter acquires a temperature in a short time and becomes a quark-gluon plasma [30–32]. Hydrodynamic models are applied to the quark-gluon plasma [33,34]. For central Pb-Pb collisions at $\sqrt{s_{NN}}=5.02$ TeV we get 0.82 GeV as the initial temperature of the quark-gluon plasma at a time of the order of 0.65 and

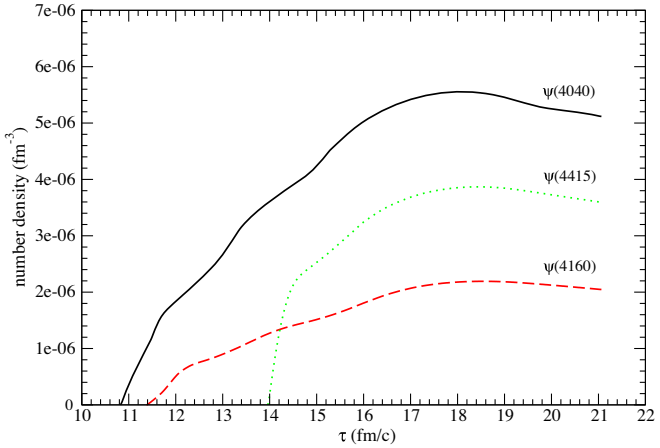

FIG. 20. Number densities as functions of τ at $r = 0$ fm.

10.05 fm/c as the proper time at which hadronization of the quark-gluon plasma occurs. We start solving the hydrodynamic equation (27) for hadronic matter at the time 10.05 fm/c with $T_c = 0.175$ GeV. Since $\psi(4040)$, $\psi(4160)$, and $\psi(4415)$ mesons are dissolved in hadronic matter when the temperature is larger than $0.97T_c$, $0.95T_c$ and $0.87T_c$, respectively, their number densities are zero above the three dissociation temperatures. From the dissociation temperatures, Eq. (26) is solved until kinetic freeze-out to get number densities that are functions of the proper time and the radius. Variation of the number densities with respect to the proper time at $r = 0$ fm is drawn in Fig. 20, and radius dependence at kinetic freeze-out is plotted in Fig. 21. Hadronic matter produced from the quark-gluon plasma expands, and its temperature decreases from the critical temperature. When the temperature arrives at $0.97T_c$, $0.95T_c$, and $0.87T_c$, production of $\psi(4040)$, $\psi(4160)$, and $\psi(4415)$ get started from reactions of charmed mesons, respectively. Therefore, when the proper time increases from 10.83, 11.38, and 13.95 fm/c, respectively, the number densities of $\psi(4040)$, $\psi(4160)$, and

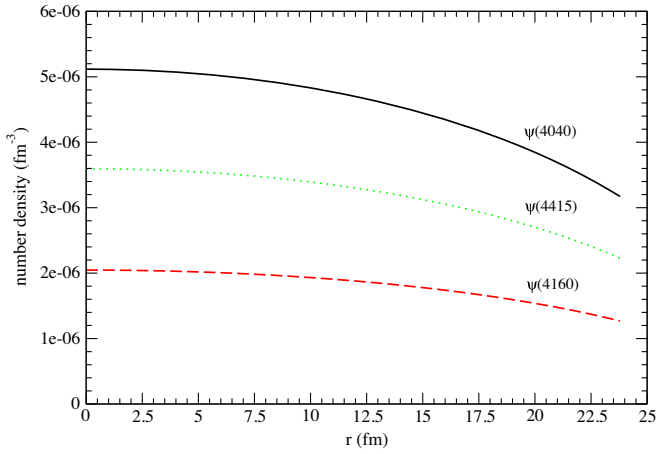

FIG. 21. Number densities as functions of r at kinetic freeze-out.

$\psi(4415)$ increase. However, the three mesons produced at $r = 0$ fm spread out, and this reduces the number densities. When the reduced amount exceeds the increased amount, the number densities decrease as seen in Fig. 20. In Fig. 21 the number densities decrease slowly when r increases from zero. From the last subsection, we have already known that at $T = 0.65T_c$, $0.75T_c$, $0.85T_c$, $0.9T_c$, and $0.95T_c$ the peak cross sections of $D\bar{D} \to \rho\psi(4040)$ $[D\bar{D}^* \to \pi\psi(4040)$, $D\bar{D}^* \to \rho\psi(4040)$, $D^*\bar{D}^* \to \pi\psi(4040)$, $D^*\bar{D}^* \to \rho\psi(4040)]$ are similar to or larger than the ones of $D\bar{D} \to \rho\psi(4415)$ $[D\bar{D}^* \to \pi\psi(4415)$, $D\bar{D}^* \to \rho\psi(4415)$, $D^*\bar{D}^* \to \pi\psi(4415)$, $D^*\bar{D}^* \to \rho\psi(4415)]$, and the latter are generally larger than those of $D\bar{D} \to \rho\psi(4160)$ $[D\bar{D}^* \to \pi\psi(4160)$, $D\bar{D}^* \to \rho\psi(4160)$, $D^*\bar{D}^* \to \pi\psi(4160)$, $D^*\bar{D}^* \to \rho\psi(4160)]$. Therefore, the number density of $\psi(4040)$ is larger than the one of $\psi(4415)$, which is larger than that of $\psi(4160)$. At kinetic freeze-out, hadronic matter has a volume of the order of 6×10^4 fm^3. As a consequence of the number densities, the numbers of $\psi(4040)$, $\psi(4160)$, and $\psi(4415)$ at kinetic freeze-out are 0.25, 0.1, and 0.18, respectively.

V. SUMMARY

We have studied the production of $\psi(4040)$, $\psi(4160)$, and $\psi(4415)$ mesons in collisions of charmed mesons in the quark interchange mechanism and space-time distribution of the three charmonia in hadronic matter created in ultrarelativistic heavy-ion collisions with the master rate equations. Formulas of the transition amplitudes are given explicitly. The temperature dependence of the quark potential, meson masses, and mesonic quark-antiquark relative-motion wave functions leads to remarkable temperature dependence of unpolarized cross sections. We have obtained the unpolarized cross sections for $D\bar{D} \to \rho R$, $D\bar{D}^* \to \pi R$, $D\bar{D}^* \to \rho R$, $D^*\bar{D} \to \pi R$, $D^*\bar{D} \to \rho R$, $D^*\bar{D}^* \to \pi R$, and $D^*\bar{D}^* \to \rho R$, where R denotes $\psi(4040)$, $\psi(4160)$, or $\psi(4415)$. In a collision of two charmed mesons, the peak cross sections of producing $\psi(4040)$ at $T = 0.65T_c$, $0.75T_c$, $0.85T_c$, $0.9T_c$, and $0.95T_c$ are similar to or larger than the ones of producing $\psi(4415)$, and the latter are generally larger than those of producing $\psi(4160)$. The numerical cross sections are parametrized so that they can be conveniently used in the master rate equations. For hadronic matter created in central nucleus-nucleus collisions, the master rate equations are given in terms of the proper time and the cylindrical polar coordinates. Below the dissociation temperatures of $\psi(4040)$, $\psi(4160)$, and $\psi(4415)$, the 21 reactions produce the three charmonia, and the master rate equations give number densities that first increase with increasing time. Among the number densities of $\psi(4040)$, $\psi(4160)$, and $\psi(4415)$, at kinetic freeze-out, the one of $\psi(4040)$ is largest and that of $\psi(4160)$ is smallest. One can find the three charmonia in the large

volume of hadronic matter created in central Pb-Pb collisions at $\sqrt{s_{NN}} = 5.02$ TeV.

ACKNOWLEDGMENTS

This work was supported by the project STRONG2020 of European Center for Theoretical Studies in Nuclear Physics and Related Areas.

APPENDIX: DERIVE THE ISOSPIN-AVERAGED CROSS SECTION

Denote the isospin of meson A (B, C, D) by I_A (I_B, I_C, I_D) and its z component by I_{Az} (I_{Bz}, I_{Cz}, I_{Dz}). Let $\phi^{I_A I_{Az}}_{A\text{flavor}}$, $\phi^{I_B I_{Bz}}_{B\text{flavor}}$, $\phi^{I_C I_{Cz}}_{C\text{flavor}}$, and $\phi^{I_D I_{Dz}}_{D\text{flavor}}$ be the flavor wave functions of mesons A, B, C, and D, respectively. $\phi^{I_A I_{Az}}_{A\text{flavor}}$ and $\phi^{I_B I_{Bz}}_{B\text{flavor}}$ are coupled to the flavor wave function $\varphi^{II_z}_{AB\text{flavor}}$ with the total isospin I and its z component I_z. $\phi^{I_C I_{Cz}}_{C\text{flavor}}$ and $\phi^{I_D I_{Dz}}_{D\text{flavor}}$ are coupled to the flavor wave function $\varphi^{I'I'_z}_{CD\text{flavor}}$ with the total isospin I' and its z component I'_z,

$$\phi^{I_A I_{Az}}_{A\text{flavor}}\phi^{I_B I_{Bz}}_{B\text{flavor}} = \sum_{II_z}(I_A I_{Az} I_B I_{Bz}|II_z)\varphi^{II_z}_{AB\text{flavor}}, \tag{A1}$$

$$\phi^{I_C I_{Cz}}_{C\text{flavor}}\phi^{I_D I_{Dz}}_{D\text{flavor}} = \sum_{I'I'_z}(I_C I_{Cz} I_D I_{Dz}|I'I'_z)\varphi^{I'I'_z}_{CD\text{flavor}}, \tag{A2}$$

where $(I_A I_{Az} I_B I_{Bz}|II_z)$ and $(I_C I_{Cz} I_D I_{Dz}|I'I'_z)$ are the Clebsch-Gordan coefficients. The isospin part of the transition amplitudes is

$$\mathcal{M}_{\text{isospin}} = [\phi^{I_C I_{Cz}}_{C\text{flavor}}\phi^{I_D I_{Dz}}_{D\text{flavor}}]^{+} P_{\text{qi}}\phi^{I_A I_{Az}}_{A\text{flavor}}\phi^{I_B I_{Bz}}_{B\text{flavor}}, \tag{A3}$$

where the symbol P_{qi} is the operator that implements quark interchange in flavor space,

$$\begin{aligned}\sum_{I_{Az}I_{Bz}I_{Cz}I_{Dz}}|\mathcal{M}_{\text{isospin}}|^2 &= \sum_{I_{Az}I_{Bz}I_{Cz}I_{Dz}}|[\phi^{I_C I_{Cz}}_{C\text{flavor}}\phi^{I_D I_{Dz}}_{D\text{flavor}}]^{+} P_{\text{qi}}\phi^{I_A I_{Az}}_{A\text{flavor}}\phi^{I_B I_{Bz}}_{B\text{flavor}}|^2 \\ &= \sum_{I'I'_z II_z}|\varphi^{I'I'_z +}_{CD\text{flavor}} P_{\text{qi}}\varphi^{II_z}_{AB\text{flavor}}|^2.\end{aligned} \tag{A4}$$

Because of isospin conservation, $I' = I$ and $I'_z = I_z$,

$$\sum_{I_{Az}I_{Bz}I_{Cz}I_{Dz}}|\mathcal{M}_{\text{isospin}}|^2 = \sum_{II_z}|\varphi^{II_z +}_{CD\text{flavor}} P_{\text{qi}}\varphi^{II_z}_{AB\text{flavor}}|^2. \tag{A5}$$

Since flavor matrix elements are independent of I_z,

$$\sum_{I_{Az}I_{Bz}I_{Cz}I_{Dz}}|\mathcal{M}_{\text{isospin}}|^2 = \sum_{I}(2I+1)|\varphi^{II +}_{CD\text{flavor}} P_{\text{qi}}\varphi^{II}_{AB\text{flavor}}|^2. \tag{A6}$$

Finally, the average over the isospin states of the two initial mesons and the sum over the isospin states of the two final mesons lead to the isospin-averaged unpolarized cross section for $A + B \to C + D$,

$$\begin{aligned}\sigma^{\text{isoav}}(\sqrt{s}, T) = &\frac{1}{(2I_A+1)(2I_B+1)} \\ &\times \sum_{I}(2I+1)\sigma^{\text{unpol}}(I, \sqrt{s}, T),\end{aligned} \tag{A7}$$

where $\sigma^{\text{unpol}}(I, \sqrt{s}, T)$ is given in Eq. (13) for the I channel.

[1] J. Siegrist *et al.*, Phys. Rev. Lett. **36**, 700 (1976); G. Goldhaber *et al.*, Phys. Lett. **69B**, 503 (1977).

[2] R. Brandelik *et al.*, Phys. Lett. **76B**, 361 (1978); Z. Phys. C **1**, 233 (1979).

[3] J. Z. Bai *et al.*, Phys. Rev. Lett. **84**, 594 (2000); **88**, 101802 (2002); M. Ablikim *et al.*, Phys. Lett. B **660**, 315 (2008).

[4] T. E. Coan *et al.*, Phys. Rev. Lett. **96**, 162003 (2006); D. Cronin-Hennessy *et al.*, Phys. Rev. D **80**, 072001 (2009); T. K. Pedlar *et al.*, Phys. Rev. Lett. **107**, 041803 (2011).

[5] G. Pakhlova *et al.*, Phys. Rev. Lett. **98**, 092001 (2007); **100**, 062001 (2008); Phys. Rev. D **77**, 011103 (2008); **80**, 091101 (2009); **83**, 011101 (2011); X. L. Wang *et al.*, Phys. Rev. D **87**, 051101 (2013); Y. L. Han *et al.*, Phys. Rev. D **92**, 012011 (2015); V. Zhukova *et al.*, Phys. Rev. D **97**, 012002 (2018).

[6] B. Aubert *et al.*, Phys. Rev. D **79**, 092001 (2009); P. del Amo Sanchez *et al.*, Phys. Rev. D **82**, 052004 (2010).

[7] M. Ablikim *et al.*, Phys. Rev. D **86**, 071101 (2012); **87**, 112011 (2013); **91**, 112005 (2015); **93**, 011102 (2016); **96**, 012001 (2017); **102**, 112009 (2020).

[8] R. Aaij *et al.*, Phys. Rev. Lett. **111**, 112003 (2013); Phys. Rev. D **102**, 112003 (2020).

[9] M. Piotrowska, F. Giacosa, and P. Kovacs, Eur. Phys. J. C **79**, 98 (2019).

[10] M. Bayar, N. Ikeno, and E. Oset, Eur. Phys. J. C **80**, 222 (2020).
[11] S. Godfrey and N. Isgur, Phys. Rev. D **32**, 189 (1985).
[12] T. Barnes, S. Godfrey, and E. S. Swanson, Phys. Rev. D **72**, 054026 (2005).
[13] J. Vijande, F. Fernández, and A. Valcarce, J. Phys. G **31**, 481 (2005); P. G. Ortega, J. Segovia, D. R. Entem, and F. Fernández, Phys. Lett. B **778**, 1 (2018).
[14] S.-T. Ji, X.-M. Xu, and H. J. Weber, Nucl. Phys. **A966**, 224 (2017).
[15] X.-M. Xu and H. J. Weber, Mod. Phys. Lett. A **35**, 2030016 (2020).
[16] T. Barnes and E. S. Swanson, Phys. Rev. D **46**, 131 (1992); E. S. Swanson, Ann. Phys. (N.Y.) **220**, 73 (1992).
[17] W.-X. Li, X.-M. Xu, and H. J. Weber, Eur. Phys. J. C **81**, 225 (2021).
[18] W. Buchmüller and S.-H. H. Tye, Phys. Rev. D **24**, 132 (1981).
[19] F. Karsch, E. Laermann, and A. Peikert, Nucl. Phys. **B605**, 579 (2001).
[20] X.-M. Xu, Nucl. Phys. **A697**, 825 (2002).
[21] M. Tanabashi *et al.* (Particle Data Group), Phys. Rev. D **98**, 030001 (2018) (and 2019 update).
[22] E. Colton, E. Malamud, P. E. Schlein, A. D. Johnson, V. J. Stenger, and P. G. Wohlmut, Phys. Rev. D **3**, 2028 (1971); N. B. Durusoy, M. Baubillier, R. George, M. Goldberg, A. M. Touchard, N. Armenise, M. T. Fogli-Muciaccia, and A. Silvestri, Phys. Lett. **45B**, 517 (1973); M. J. Losty, V. Chaloupka, A. Ferrando, L. Montanet, E. Paul, D. Yaffe, A. Zieminski, J. Alitti, B. Gandois, and J. Louie, Nucl. Phys. **B69**, 185 (1974); W. Hoogland *et al.*, Nucl. Phys. **B126**, 109 (1977).
[23] S. D. Protopopescu, M. Alston-Garnjost, A. Barbaro-Galtieri, S. M. Flatté, J. H. Friedman, T. A. Lasinski, G. R. Lynch, M. S. Rabin, and F. T. Solmitz, Phys. Rev. D **7**, 1279 (1973); B. Hyams *et al.*, Nucl. Phys. **B64**, 134 (1973); P. Estabrooks and A. D. Martin, Nucl. Phys. **B79**, 301 (1974); V. Srinivasan *et al.*, Phys. Rev. D **12**, 681 (1975); L. Rosselet *et al.*, Phys. Rev. D **15**, 574 (1977); C. D. Froggatt and J. L. Petersen, Nucl. Phys. **B129**, 89 (1977); A. A. Bel'kov, S. A. Bunyatov, K. N. Mukhin, O. O. Patarakin, V. M. Sidorov, M. M. Sulkovskaya, A. F. Sustavov, and V. A. Yarba, JETP Lett. **29**, 597 (1979); E. A. Alekseeva, A. A. Kartamyshev, V. K. Makar'in, K. N. Mukhin, O. O. Patarakin, M. M. Sulkovskaya, A. F. Sustavov, L. V. Surkova, and L. A. Chernysheva, Sov. Phys. JETP **55**, 591 (1982); R. García-Martín, R. Kamiński, J. R. Peláez, J. R. de Elvira, and F. J. Ynduráin, Phys. Rev. D **83**, 074004 (2011).
[24] S.-T. Ji, Z.-Y. Shen, and X.-M. Xu, J. Phys. G **42**, 095110 (2015).
[25] Z.-Y. Shen, X.-M. Xu, and H. J. Weber, Phys. Rev. D **94**, 034030 (2016).
[26] H. Niemi, K. J. Eskola, and R. Paatelainen, Phys. Rev. C **93**, 024907 (2016).
[27] Y.-J. Liu, X.-M. Xu, and Y.-Q. Li, Chin. Phys. C **32**, 733 (2008).
[28] F. Cooper and G. Frye, Phys. Rev. D **10**, 186 (1974).
[29] S. Acharya *et al.*, J. High Energy Phys. 10 (2018) 174.
[30] X.-M. Xu, J. Phys. Conf. Ser. **458**, 012021 (2013).
[31] X.-M. Xu, in *Proceedings of XXXth International Workshop on High Energy Physics*, edited by V. Petrov and R. Ryutin (World Scientific, Singapore, 2015).
[32] X.-M. Xu, Z.-Y. Shen, Z.-C. Ye, and W.-J. Xu, Phys. Rev. C **87**, 054904 (2013).
[33] W. Florkowski, *Phenomenology of Ultra-Relativistic Heavy-Ion Collisions* (World Scientific, Singapore, 2010).
[34] R. Ryblewski, J. Phys. G **40**, 093101 (2013).